Martin Øvsthus

Characterization of the Somatostatin cell population in the Medial Entorhinal Cortex of the Mouse

Master's thesis in Neuroscience
Supervisor: Bente Jacobsen, MSc
Trondheim, June 2016

Norwegian University of Science and Technology
Faculty of Medicine
Kavli Institute for Systems Neuroscience / Centre for Neural Computation

NTNU
Norwegian University of
Science and Technology

Acknowledgements

The work presented in this thesis was performed at the Kavli Institute for Systems Neuroscience/Centre for Neural Computation at the Norwegian University of Science and Technology (NTNU), under the supervision of PhD candidate Bente Jacobsen.

I would especially like to thank my supervisor Bente Jacobsen for believing in me and for all her help, advice and guidance through this project. I would like to thank Prof. Menno Witter who gave me the opportunity to do this project. Thanks also belong to Bruno Monterotti for all the jokes, laughs and always being helpful with technical matters. For the rest of the Witter group, thank you for being supportive.

To my good friend Gjermund, thank you for all the laughs, discussions and for keeping me sane throughout this project. I would also like to thank my family and friends for encouraging and supporting me during my studies.

Abstract

The medial entorhinal cortex receives converging input from the hippocampal formation, the parahippocampal region and multiple neocortical and subcortical regions. Since the discovery of spatially modulated cells, the medial entorhinal cortex is suggested to have a strong functional role in spatial navigation. In the process to illuminate the mysteries of the underlying spatial circuitry, a lot of attention has been directed toward the cell populations residing in the medial entorhinal cortex. Interneurons are indicated to have an important role in modulation of the local principal cells in cortical networks. However, in the medial entorhinal cortex, little is known about the different interneuron population.

The aim of this thesis was to describe the distribution and monosynaptic inputs to the somatostatin cell population of the medial entorhinal cortex, as well as optimizing the viral tracing protocol. To characterize the distribution of somatostatin cells, an adeno-associated virus helper virus was injected into the medial entorhinal cortex of somatostatin-Cre mice. To visualize monosynaptic tracing, somatostatin-Cre mice were injected with adeno-associated virus helper virus, followed by an incubation period and injection of EnvA G-deleted rabies virus. The brains were cut in the horizontal plane and cortical areas were delineated based on Nissl stains with Cresyl Violet. Adeno-associated virus helper virus and rabies virus fluorescent expression were immunohistochemically enhanced with AlexaFluor® dyes, and the viral expression was analyzed with confocal microscopy.

I tested multiple viral tracing protocols and the results showed that in order to receive optimal monosynaptic transport, the monosynaptic tracing method worked better in case of moderate to large injections with high titer virus. Immunohistochemical analyzes showed that the SST cell population was confined to deep layers of the MEC, whereas local monosynaptic labelled rabies cells were confined to and projected to superficial layers. Long-distance labelled cells were observed in the hippocampal formation, the parahippocampal region, the retrosplenial cortex and the medial septum. The results indicate that the somatostatin cells mainly receive inputs to starter cells in superficial layers. Long-distant monosynaptic transport show that the medial entorhinal cortex received stronger input from the parahippocampal region and the hippocampal formation than from neocortical and subcortical structures.

Contents

Abbreviations

AAV	Adeno-associated virus
CA1	Cornu Ammonis 1
CA2	Cornu Ammonis 2
CA3	Cornu Ammonis 3
DG	Dentate Gyrus
EC	Entorhinal cortex
GABA	γ-aminobutyric acid
GFP	Green Fluorescent Protein
HA	Influenza hemagglutinin
HF	Hippocampal formation
IHC	Immunohistochemistry
LEC	Lateral Entorhinal Cortex
LSI	Lateral septal nucleus, intermediate part
MC	Martinotti cells
MEC	Medial Entorhinal Cortex
MnPO	Median Preoptic nucleus
NSAID	Non-steroidal Anti-inflammatory drug
PaS	Parasubiculum
PER	Perirhinal Cortex
PFA	Paraformaldehyde
PHR	Parahippocampal region
POR	Postrhinal Cortex
PrS	Presubiculum
PV	Parvalbumin
RSC	Retrosplenial Cortex
SHy	Septohypothalamic nucleus
SST	Somatostatin
Sub	Subiculum
Tris	Tris(hydroxymethyl)aminomethane

Chapter 1 Introduction

The hippocampal formation (HF) and the neighboring parahippocampal region (PHR) have an anatomical organization that is largely conserved across species, giving scientists the opportunity to deduce knowledge from animal models to humans (Amaral & Lavenex 2007). In early pioneering work, the HF and the PHR had already established a functional role in the processes of memory and learning (Scoville & Milner 1957). Until the discovery of place cells, there was no behavioral experimental paradigm available to test these hypotheses in animal models (O'Keefe & Dostrovsky 1971; O'Keefe 1976). These cells fire when an animal is moving in specific locations in space (O'keefe 1976), thus, providing a reliable behavioral paradigm to study the neuronal circuits of the HF. Other spatially modulated cells were later found in the medial entorhinal cortex (MEC), including the grid cells, border cells and head-direction cells (Taube 1998; Hafting et al. 2005; Sargolini et al. 2006; Solstad et al. 2008). The discovery of these functional cell types established an important role for the MEC in relation to spatial navigation. Furthermore, they have later been found to be consistent across phylogenetically distant species (Yartsev et al. 2011; Killian et al. 2012). Thus, it is presumed that the basic connectivity and functional properties of these cell types are the same in humans as in animals (Doeller et al. 2010).

The functional properties of the spatially modulated cells have received much attention. This have in turn prompted investigations into which cell populations residing in the MEC correlate with which functional properties (Klink & Alonso, 1997; Canto et al. 2008; Canto & Witter 2012). Although, a large part of the attention has been directed toward the principal cell population, recent evidence elucidates the importance of interneuron connectivity for grid cell firing in the local circuitry (Couey et al. 2013; Pastoll et al. 2013). Moreover, new findings have shown that the local interneurons have preferential connectivity with principal cell types in LII of the MEC (Fuchs et al. 2016). However, it is unclear how this may affect the functional properties of spatial cells. Despite a growing interest to cells in the MEC, not much is known about the intrinsic wiring and individual cell groups extrinsic inputs. Thus, in order to understand the functionality of this complex system to its full extent, it is important to decipher the microcircuitry of the MEC.

1.1 Axes of the parahippocampal region and the hippocampal formation

The HF consists of several substructures, the dentate gyrus (DG), the subregions of cornu ammonis (CA1, CA2 and CA3) and the subiculum. The PHR consists of the presubiculum (PrS), the parasubiculum (PaS), the MEC, the lateral entorhinal cortex (LEC), the perirhinal cortex (PER) and the postrhinal cortex (POR; Cappaert et al. 2015). An overview of all the substructures are found in figure 1. In rodents, the HF has a curved appearance, looking like a large C-shaped structure. It is situated in the caudal part of the brain, extending from the dorsal basal forebrain septal nuclei to the ventral amygdaloid nuclei. This longitudinal axis is referred to as the septotemporal axis, extending from top to bottom in the brain. The transverse axis is perpendicular to the septotemporal axis. It is termed the proximodistal axis with the dentate gyrus at the proximal end (Cappaert et al. 2015).

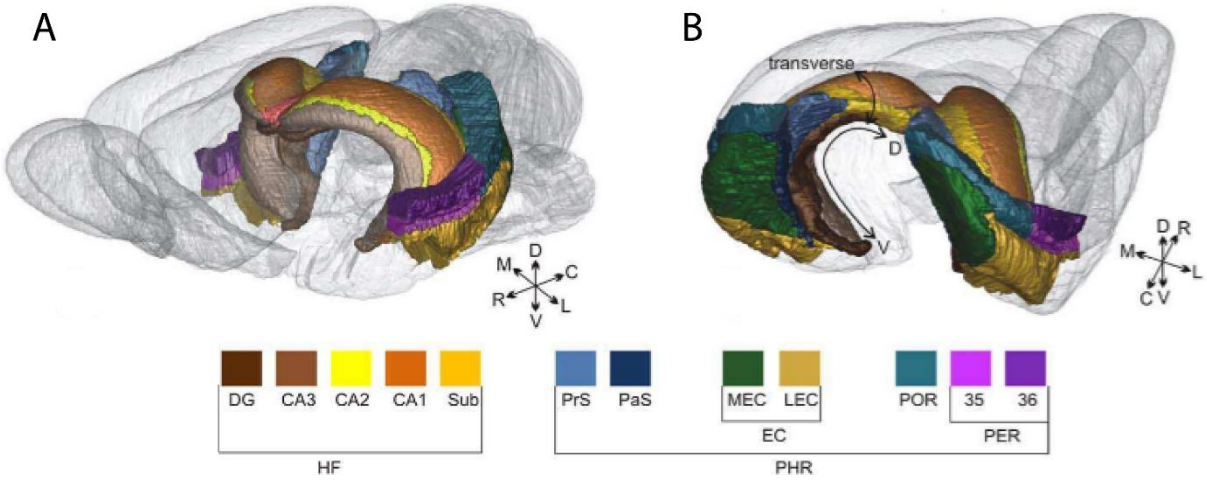

Figure 1. **Overview of the hippocampal region in the cerebral hemispheres of the rat.** A) Oblique frontal view. B) Oblique rear view. Colors indicate the different regions in the hippocampal formation and the parahippocampal region. Adapated from Boccara et al. 2015. For abbreviations, see list of abbreviations.

The parahippocampal region wraps around large portions of the HF. The longitudinal axis of the PHR is referred to as the dorsoventral axis, analogous to the septotemporal axis of the HF (Figure 1). The transverse axis is termed the mediolateral axis, where the medial parts sit in the region closest to the HF, while the lateral part is the region closest to the rhinal fissure (Cappaert et al. 2015).

1.2 The medial entorhinal cortex

The entorhinal cortex (EC) is a part of a highly interconnected microcircuit with prominent topographical organizations. Information from multiple modalities in the brain converge in the EC before being passed through the HF where the information is updated and relayed back to the cortical mantle through the entorhinal cortex (van Strien et al. 2009; Cappaert et al. 2015).

The MEC is one of two subregions in the EC. It is situated in the ventrocaudal convexity of the rodent brain. It has been described as periallocortex, which is a transition between the three-layered allocortex and six-layered neocortex (Cappaert et al. 2015). The generally accepted laminar organization divides the EC in two acellular layers, LI and lamina dissecans, and four cellular layers, LII-LIII and LV-LVI (Insausti et al. 1997). The outermost LI is cell sparse, but rich in fibers. In LII there are found medium to large sized stellate and pyramidal cells (Canto et al. 2008), with stellate cells being the most abundant cell type (Klink & Alonso 1997). The cells are usually arranged in a continuous manner giving the appearance of a homogenous layer (Insausti et al. 1997). LIII is more heterogeneous in its appearance, with cells in different sizes and shapes. It is mainly comprised of pyramidal and multipolar cells (Cappaert et al. 2015). The lamina dissecans (LIV) comprises only a few cells. LV consists of medium to large sized pyramidal cells, often recognized by a looser arrangement, and LVI is recognized by being heterogeneous in its appearance, inhabited by cells of different sizes and shapes. Both LV and LVI is recognized by their radial arrangement of cells, usually more prominent in LV (Insausti et al. 1997; Canto et al. 2008). For a detailed description of the cytoarchitecture of the MEC, see paragraph 2.4, “Delineation of monosynaptic input structures”.

1.2.1 The intrinsic connectivity and input of the medial entorhinal cortex

The MEC has a distinct intrinsic connectivity as well as connections with the HF, the PHR, and a number of cortical and subcortical regions (Cappaert et al. 2015). Afferents to the MEC are strictly topographically arranged both across the dorsoventral and mediolateral axes, but also across the different laminae. In the two following sections the intrinsic connectivity and the extrinsic inputs to the MEC will be described.

1.2.2 Intrinsic connectivity

The intrinsic connectivity of the MEC comprises connections along the dorsoventral, mediolateral and radial axes. The interconnectivity is preferably organized along the

dorsoventral axis, showing a rather restricted mediolateral distribution (Köhler 1986; Dolorfo & Amaral 1998). Connectivity along the radial axis is also more restricted. The projections from neurons in the superficial layers, LII and LIII, are limited to the superficial layers and do not or only sparsely target deep layers. However, the deep layers project extensively to superficial layers (Köhler 1986). Axons of cells in LV terminate on principle cells and interneurons in LI-LIII, and the projections are largely excitatory (95%; van Haeften et al. 2003). The principal cells residing in LII of the MEC have been shown have preferential connectivity with interneuron subpopulations, and only to a limited extent directly to each other (Couey et al. 2013; Fuchs et al. 2016)

1.2.3 The inputs to the medial entorhinal cortex

The hippocampal formation

The MEC has strong reciprocal connectivity with the HF (Agster & Burwell 2013). Together with structures in the PHR the HF is the source of almost half the afferent inputs to the MEC (Kerr et al. 2007). The major afferents to the MEC originate in the CA1 and the subiculum (Cappaert et al. 2015). Both substructures are known to preferentially target LV of the MEC, however, LIII also receives weak terminations (Kloosterman et al. 2003; Cenquizca & Swanson 2007). The inputs from the HF are topographically organized such that the septal CA1 and subiculum project to the dorsal MEC. Conversely, the temporal CA1 and subiculum project to the ventral MEC (Agster & Burwell 2013). Topographical organization is also displayed along the transverse axis. The proximal CA1 and the distal subiculum projects to the MEC, while the distal CA1 and proximal subiculum are largely connected to the LEC (Kleinknecht 2003). A small projection to the MEC from the HF also originates in the CA2, this is thought to preferentially target LII cells (Rowland et al. 2013).

The parahippocampal region

The MEC receives inputs from all other structures in the PHR, the different inputs terminate with different strengths and in different layers (Agster & Burwell 2013). The inputs from the PrS and the PaS have been found to target all layers in the MEC (Canto et al. 2012). However, they do target some layers more extensively than others. The PrS favors LI and LIII (Caballero-Bleda & Witter 1994) as well as targeting LV (Wouterlood et al. 2004). The PaS preferentially targets LII of the MEC (Caballero-Bleda & Witter 1993). All regions of the POR provide inputs to LI and LIII in the MEC, preferentially to the dorsal and caudal regions (Burwell & Amaral

1998a; Burwell & Amaral 1998b). Afferents are also provided by the PER, however, this connection is weak compared to the POR (Burwell & Amaral 1998b; Agster & Burwell 2013). The interconnectivity between the two entorhinal subregions is strong, and the LEC provides inputs to almost all layers of the MEC (Dolorfo & Amaral 1998).

Neocortical and subcortical structures

The MEC has connectivity with many neocortical and subcortical structures (Burwell & Amaral 1998a; Kerr et al. 2007; Agster & Burwell 2009; Agster & Burwell 2013). Approximately one-fifth of the afferent input to the MEC originates in neo- or paleocortical structures (Kerr et al. 2007). The piriform cortex provides the most extensive input to the MEC. However, this projection preferentially targets intermediate and ventral regions of the MEC, providing the dorsal MEC with little input (Burwell & Amaral 1998a; Kerr et al. 2007). Moderate projections arise in the frontal regions, preferentially from motor areas (Burwell & Amaral 1998a). These projections mainly target the region close to the PaS (Kerr et al. 2007). The retrosplenial cortex (RSC) provides the heaviest input from the cingulate cortex, and it targets the deep layers of the MEC (Jones & Witter 2007).

Kerr et al (2007) reported that roughly one-third of the inputs to the MEC are found in subcortical regions, indicating that subcortical projections have a substantial influence on the MEC. The main subcortical inputs originate in the claustrum, the amygdala and the thalamus (Kerr et al. 2007), as well as in the medial septal nucleus (MS) particularly in the vertical limb of the nucleus of the diagonal band of Broca (Alonso et al. 1984). Projections from the MS consist of glutamatergic, GABAergic and cholinergic neurons and target all layers of the MEC (Kondo & Zaborszky 2016), but LII and the lamina dissecans receive stronger inputs than the other laminae (Alonso et al. 1984).

1.3 Interneurons

The brain consists of different classes of neurons that carry out specific functions and process information before it is sent between different areas. The major neuronal subgroups are excitatory projection neurons and inhibitory interneurons. Projection neurons make up 75-85% of the total cell population and use glutamate as their neurotransmitter (Harris & Mrsic-Flogel 2013). Inhibitory interneurons constitute a smaller population, only contributing to 15-25% of the total cell population. The majority of interneurons use γ-aminobutyric acid (GABA) as their main neurotransmitter(Ren et al. 1992; Beaulieu 1993). Despite their low numbers, inhibitory

neurons are of pivotal importance for neural networks. They form a heterogeneous cell population with diverse morphologies, electrophysiological and molecular properties. Their axons, although locally confined, have extensive arborizations that innervate cells near to them to a considerable extent. Despite being very heterogeneous, some general features are shared and set them apart from principal cells. Most mature interneurons have aspiny dendrites; both excitatory and inhibitory synapses are located on their somata, and their axons are locally projecting, either within their layer or across multiple columns, but usually not between gross anatomical regions (Markram et al. 2004). Based on the diverse properties, one can subdivide them into a plethora of different groups that influence the target cells in multiple ways (Freund & Buzsáki 1996; Wang et al. 2004; Yuste 2005; Ascoli et al. 2008; DeFelipe et al. 2013)

The large diversity of GABAergic interneurons gives them the ability to control information flow to specific domains on principal cells, thereby altering the spatiotemporal processing of information. They do this by controlling the timing of principal cell firing, filtering inputs, synchronizing network activity, and generating cortical rhythms. Furthermore, inhibition responds to dynamic changes in excitation, opening for increased dynamic range in cortical circuits, sensory receptive fields and plasticity control and preventing runaway excitation in the cortical loops (Markram et al. 2004; Rudy et al. 2011).

1.3.1 Interneuron diversity and classification

Due to the large diversity of GABAergic interneurons, there has been a need for a good classification system. Multiple attempts to classify interneurons based on their morphological, biochemical and electrophysiological properties have been made. Depending on the type of study being performed, different classification strategies may be employed in order to understand how different groups of interneurons are integrated in the cortical networks (Markram et al. 2004; Yuste 2005; Ascoli et al. 2008; Rudy et al. 2011; DeFelipe et al. 2013).

Morpholocial classification

Traditionally, dendritic morphologies have been used to classify the morphology of principal cells in the cortex. However, the dendrites of interneurons have turned out to be so diverse that it is impossible to categorize them on the basis of this feature. Thus, axonal arborizations of interneurons have been considered the best way to identify different groups of interneurons (Markram et al. 2004; Ascoli et al. 2008). By dividing the interneurons according to axonal targets it is possible to get a reasonable idea of their functions. In the neocortex, where most of

these classifications have been worked out, interneurons can be grouped into axon-targeting, soma- and proximal dendrite-targeting, dendrite-targeting and distal dendrite and tuft-targeting interneurons (Ascoli et al. 2008). Axo-axonic interneurons or chandelier cells are located in LII-LVI. These cells have axonal trees reminiscent of chandeliers with dense axonal bundles that wrap around the axon initial segments of principal cells (Markram et al. 2004). Soma- and proximal dendrite targeting interneurons are typically basket cells that wrap basket like axonal arborizations around the somata of pyramidal cells. Their unique placement make them suitable to strongly influence the output of the pyramidal neurons that they innervate (Wang et al. 2002; Markram et al. 2004). Dendrite-targeting cells contain a rather diverse group of cells, double bouquet cells, bipolar cells and bitufted cells. Double bouquet cells are found in LII-LV, while bipolar cells and bitufted cells are found in all layers but LI (Markram et al. 2004; Druga 2009). Distal dendrite and tuft-targeting interneurons mainly consist of the martinotti cell (MC). They are located through LII-LVI, and can be recognized by widely extending axonal projections that ascend from the soma to superficial cortical layers. Typically the boutons of the axons have a spine-like appearance (Wang et al. 2004; Silberberg & Markram 2007).

Biochemical classification

Different biochemical markers can be used to differentiate classes of interneurons. Three large non-overlapping interneuron populations have been described on the basis of such markers; cells that express the Ca^{2+} binding protein parvalbumin (PV), cells that express the neuropeptide somatostatin (SST) and cells that express the biochemical marker for the ionotropic serotonine receptor 5HT3a (Lee et al. 2010; Rudy et al. 2011), a receptor that previously had been known to be expressed exclusively in GABAergic neurons (Morales & Bloom 1997). The 5HT3a cell group likely contains other subgroups of cells such as the vasoactive intestinal peptide (VIP) expressing cells. Together the PV, SST and 5HT3a expressing interneuron groups have been suggested to make up 100% of the interneuron population in the cortex, ~40% of the cells being PV neurons, ~30% SST neurons and ~30% 5HT3a neurons (Rudy et al. 2011).

1.3.2 Interneurons expressing the neuropeptide somatostatin

Interneurons expressing the neuropeptide SST have been found throughout all layers of the neocortex (Lee et al. 2010). This biochemical marker has been seen in basket cells (Jiang et al. 2015; Nassar et al. 2015), bitufted cells (Markram et al. 2004) and MCs (Wang et al. 2004). Of these morphological subtypes, only the MCs have been found to exclusively express SST,

whereas the other cell groups may express other markers such as PV and VIP (Wang et al. 2004).

MCs are the largest group of SST cells in the neocortex, and they make up about 15% of the total interneuron population in any neocortical area (Druga 2009). The MCs have a unique morphological phenotype. The somata are ovoid or spindle shaped, and they are located in LII-LVI in the cortex. Their dendrites usually have elaborate bitufted morphologies that that stretch into adjacent layers. MCs axons bear a characteristic appearance as they always extensively innervate layer I of the cortex, spreading processes both within and across multiple cortical columns. They are thought to be the only interneuron type to provide extensive cross-column inhibition (Wang et al. 2004; Jiang et al. 2015). Regarding electrophysiological properties, the MCs are usually described as low-threshold spiking interneurons. The depolarization of the MCs gets stronger by more excitatory input, thus, exerting stronger inhibition with more excitatory input (Kawaguchi and Kubota, 1997; Wang et al. 2004; Silberberg and Markram, 2007).

MCs have been found to provide input to almost all other cell types within the reach of their axons (Jiang et al. 2015), and thus provide widespread inhibition within a brain area. Despite their rather non-specific output properties, the majority of their local input originates from pyramidal cells within the column where they are located (Silberberg and Markram, 2007; Jiang et al. 2015). Inputs from pyramidal cells drive MCs to inhibit tuft-dendrites of other pyramidal cells. Thus, pyramidal cells can inhibit the activity of surrounding pyramidal cells through MCs (Figure 2; Kapfer et al. 2007; Silberberg & Markram 2007; Berger et al. 2010). This is thought to be part of a filtering mechanism of excitatory inputs to pyramidal cells by inhibiting their tuft-dendrites. By doing this, nearby columns will be inhibited by MCs, which will create stronger excitation on the initial pyramidal cell (Berger et al. 2010). Furthermore, MCs have been found to exhibit this mechanism in multiple neocortical regions (Berger et al. 2009).

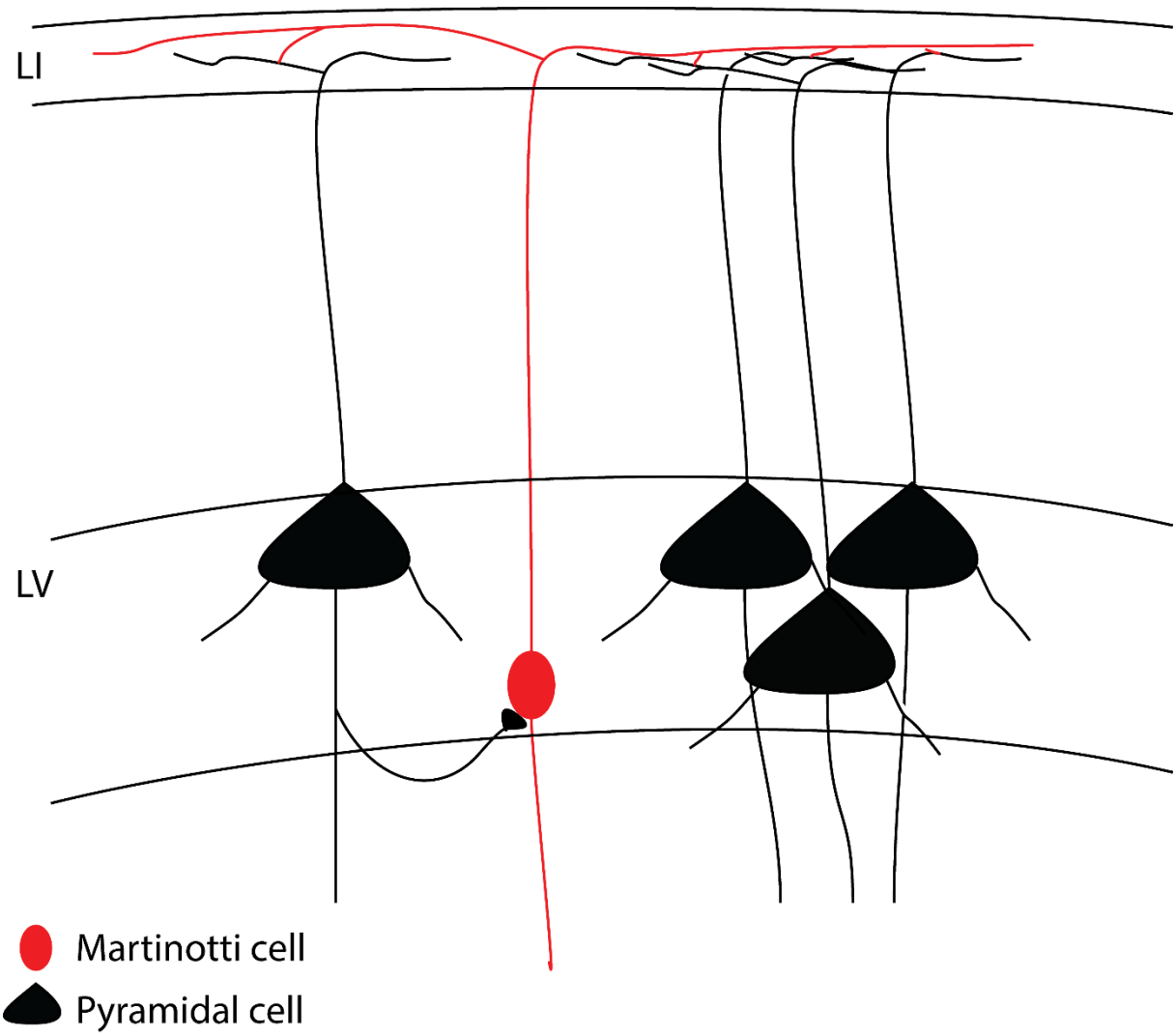

Figure 2. **Illustrating the connectivity made by the Martinotti cell.** Pyramidal cells synapse onto martinotti cells. The martinotti cell axons branches extensively in LI, inhibiting surrounding pyramidal cells. The pyramidal cells will indirectly influence its own input. Based on Silberberg & Markram (2007) and Berger et al. (2010).

1.3.3 Somatostatin expressing cells in the medial entorhinal cortex

The networks of interneurons in the MEC have received little attention until recently. There are a few immunohistochemical studies looking at SST cells in the area, however these studies show conflicting results, reporting more cells in either superficial layers (Wouterlood & Pothuizen 2000), or in deep layers (Köhler & Chan-Palay 1983). Thus, there are inconsistent reports about which layers contain the majority of SST cells. However, reports from the somatosensory cortex (Morrison et al. 1983) and the PrS (Nassar et al. 2015) indicate that the SST cells tend to be preferentially distributed in deeper parts of the cortex, and that a large portion of the cells have morphological features that are typical for MCs. One recent study also

looked at the connectivity of interneurons in LII of the MEC, this work showed that SST cells in LII of the MEC are connected reciprocally to some but not all principal cell types within the layer. This suggests that SST cells make specific connections to designated partners within their local networks. The firing pattern of recorded SST cells were found to be low-threshold firing (Fuchs et al. 2016).

1.4 Neuroanatomical tracing with rabies virus and helper virus

Understanding the organization of the brain has been aided by the emergence of recombinant viral vectors. Monosynaptic circuit tracing is a relatively new method in the repertoire of neuroanatomical tracing tools, and is potentially a powerful method for mapping out neuronal circuits (Wall et al. 2010; Sun et al. 2014; Wall et al. 2016). By using pseudotyped rabies viruses and adeno-associated virus (AAV) helper viruses with cell-type specific Cre-driver lines, it is possible to trace inputs to specific subsets of starter cells in a network (Callaway & Luo 2015; Ghanem & Conzelmann 2016). An overview of monosynaptic tracing can be found in figure 3.

1.4.1 Cre-recombinase and its function

Cre-recombinase is an enzyme that catalyzes recombination between specific DNA sites, known as loxP sites. It will catalyze these DNA sequences, thereby fusing two DNA sites upon its removal (Nagy 2000). A way to picture it is to imagine Cre-recombinase as a scissor that cuts out the loxP sites, joining the DNA that was separated by loxP. However, it is not expressed naturally in mammals. Therefore, transgenic mouse lines that express this enzyme have to be made. Cre-recombinase can be introduced to be expressed in all tissues, or a specific tissue or cell type (Kos 2004). This creates a very specific expression, exploited in monosynaptic tracing.

1.4.2 Adeno-associated helper virus and Cre-dependence

AAV vectors have been extensively used in gene therapy (Grieger & Samulski 2005), but are also popular vectors to use in neurobiology (Callaway & Luo 2015). It is a member of the parvovirus family, and one of the smallest DNA viruses. The limited size is an disadvantage as it limits the number of base pairs that it can carry, thus limiting its “payload” capacity (Skubis-Zegadło et al. 2013). However, AAV vectors may be tailored to only express their gene package in cells expressing Cre-recombinase. The AAV helper virus used to insert the genes for the rabies tracing experiments are made to express the TVA receptor, the G-protein and a molecular

tag for identifying starter cells. By combining the Cre-dependence of the AAV helper viruses with the retrograde transport capabilities of the pseudotyped G-deleted rabies virus, one can get virus expression in a very specific subset of cells and trace their inputs (Wall et al. 2010).

1.4.3 EnvA-pseudotyped G-deleted rabies virus

Rabies virus is a neurotropic virus in the *rhabdoviridae* family. Its wild type causes one of the most lethal zoonotic diseases, usually ending in fatal encephalomyelitis (Ghanem & Conzelmann 2016). Due to its extreme neurotropism and the way in which it is transported within and between cells, genetically engineered rabies viruses can be exploited for neuroanatomical tracing. Once a rabies virus infects the nervous system, it travels in a retrograde manner from the axon to the cell body of the infected cell, where it can access the necessary proteins for replication, assembly and release. The G-protein coating the rabies virus surface is an important structural component. After translation, the G-proteins are transported and embedded in the host cell membrane, thereby coating the membrane of the rabies virus as it is released from the neuronal cell. The G-protein gives the rabies virus the ability to infect presynaptic terminals of synaptically connected cells (Schnell et al. 2009; Ghanem & Conzelmann 2016).

A wild-type rabies virus will non-specifically spread to nearby cells, and transfer across multiple synapses depending on the time it is given (Callaway & Luo 2015). In this way rabies virus can be used to trace neural circuits. Novel genetic engineering techniques have however made it possible to pseudotype the rabies virus by deleting the G-protein and coating the virus with an envelope protein that is receptor dependent. In this way the rabies can be made to specifically target only subsets of cells within a network by using cell type specific Cre-driver lines (Callaway & Luo 2015). Moreover, this system makes it possible to restrict the synaptic transfer to only cells that are monosynaptically coupled to the primary infected cells.

For experiments in mammals, the G-protein is usually replaced by the envelope protein type A from the avian sarcoma leukosis virus (EnvA). It specifically targets TVA receptors, not found in mammalian neurons. Cell populations can be engineered to express TVA receptors, thus, creating a specific set of neurons that the pseudotyped rabies virus can enter. A fluorescent marker typically accompanies the genetic modifications such that rabies infected cells can be identified (Callaway & Luo 2015).

1.4.4 Monosynaptic tracing

In order to carry out monosynaptic tracing experiments with the system described above, focal injections of virus are made in the area of interest in a mouse line expressing Cre-recombinase in the cell type of interest. First, the Cre-dependent AAV helper virus infects cells in the designated area. Due to the functional properties of Cre-recombinase, the AAV helper virus will only be able to express its gene package in cells that are Cre-positive (Callaway & Luo 2015). The TVA receptor and the G-protein are expressed in Cre-positive cells within a couple of weeks. Since the rabies virus is pseudotyped with EnvA, specific for the TVA receptor, it enters cells with TVA receptors and express its tag in these cells. The rabies virus seems able to enter cells that express only a few TVA receptors (Seidler et al. 2008), and only a single rabies viral particle is sufficient to infect the cell (Haberl. et al. 2015). The rabies virus will express its marker in the cytosol of the infected cells, and the virus will replicate here. The new rabies viruses will have their membranes coated by G-proteins because the AAV has carried the genes for the expression of this. This will make the rabies virus able to infect presynaptic terminals of input cells, and show the monosynaptic projections to the starter cells (Wall et al. 2010; Callaway and Luo, 2015). Following this method, the starter population will be filled with both the AAV helper virus marker and the maker carried by the rabies virus, while monosynaptic cells will only be filled with the marker express by rabies virus. Figure 3 show an overview of the process explained in the abovementioned text.

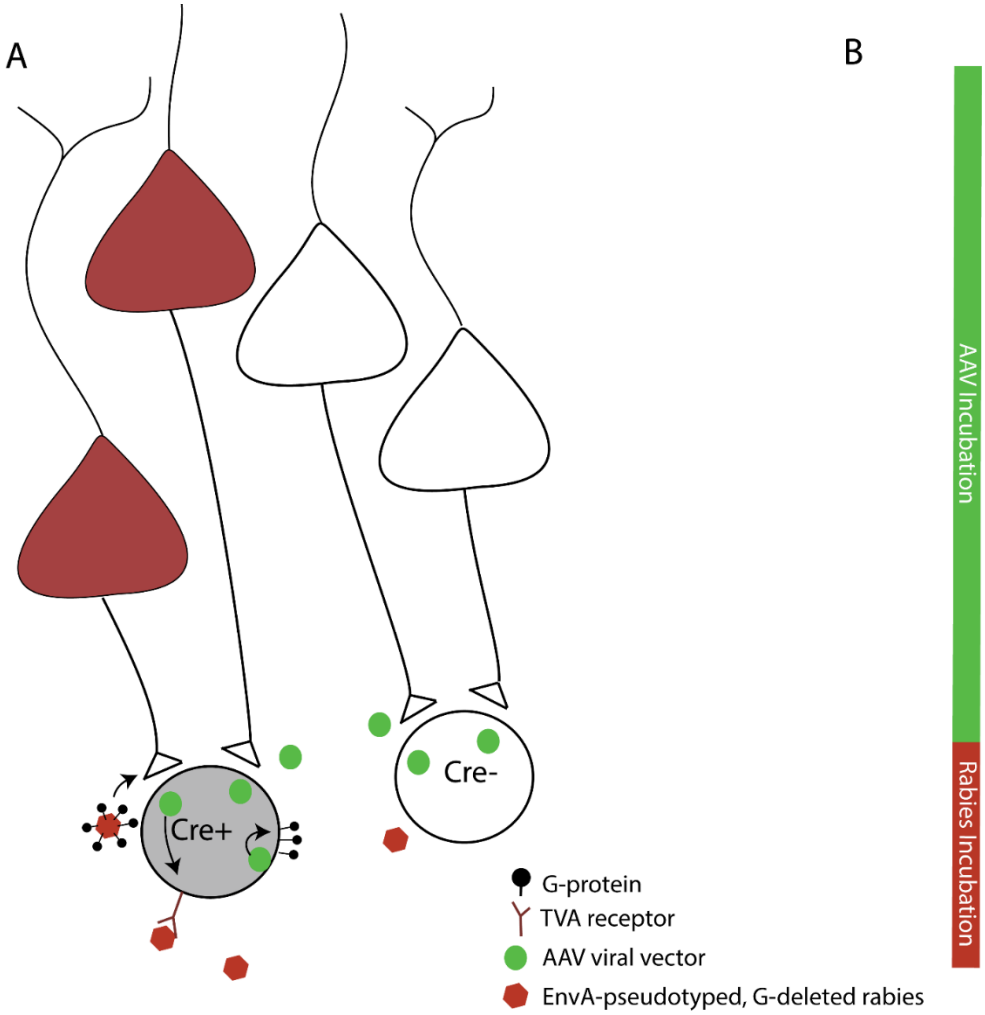

Figure 3. **Description of the monosynaptic tracing system.** A) Show an overview of the monosynaptic tracing system described in the text. Cre-positive cells are infected by AAV, expressing genes for TVA-receptors and G-protein. G-protein and TVA-receptors are transported to the cell surface and rabies virus can enter the cell to replicate. Rabies virus coated in G-proteins buds from the cells and jumps to the presynaptic synapse. The grey cell illustrates a starter cell. B) AAV viral vector and rabies virus are separately injected.

1.5 Aim

The aim of this thesis was to describe the distribution of SST cells in the MEC of mice using immunohistochemistry. I also aimed to characterize the monosynaptic inputs to SST cells in the MEC. In order to do this, I used a transgenic mouse line and a retrograde monosynaptic tracing system taking advantage of genetically engineered viral vectors. I thus also wanted to characterize the specificity of the mouse line, and test different strategies using the monosynaptic tracing system in order to optimize our technique.

Chapter 2 Materials and methods

2.1 General procedures

2.1.1 Animals

A total of 9 adult animals of both genders of the SST-Cre (Ssttm2.1(Cre)Zjh/Jax) transgenic mouse-line (Taniguchi et al. 2011) 20-35g were used for this study. They were in-house bred, originating from Jackson Laboratories. Animals were kept in a standardized environment (*12hr* reversed Day/Night cycle, 21 ± 1°C, 60% RH) with free access to water and food. All animals used in this study were raised and handled according to regulations and laws provided by The Norwegian Research Authority (Forsøksdyrutvalget). List of animals and their use in experiments can be found in Appendix I.

2.1.2 Anaesthesia and analgesia

Anaesthesia of animals was induced in an induction chamber filled with surgical air containing 4% isoflurane, flowing at 1L per minute. After induction, the animals were moved to a surgical mask where the anaesthesia was maintained at a deep level throughout the surgery, and adjusted according to breathing frequency. For pain relief, the NSAID Rimadyl (50 *mg/ml*, 1:50 dilution, 5 mg/kg) and the opioid Temgesic (0.3 *mg/ml*, 1:10 dilution, 0.05-0.1 mg/kg) was injected subcutaneously after the induction of anaesthesia. The local anaesthetic Marcain (2.5 *mg/ml*, 1:5 dilution, 1 mg/kg) was injected at the site of surgical intervention 15 min prior to the incision. In order to alleviate post-operative pain Rimadyl was administered the day after surgery.

2.1.3 Surgical procedure

Prior to surgery, animals were weighed before being put under anaesthesia. The analgesics were injected, and the level of anaesthesia was monitored by checking the animal's reflexes and by observing their breathing patterns. The animals were mounted and fixed in a stereotactic frame (David Kopf Instruments, USA) and Simplex (Tubilux Pharma S.p.A., Italy) was applied to avoid the mouse's eyes from drying out. Ear bars positioned at the bones in the ear cavity were used to fix the animal's head position in the frame. Subsequently, the surgical area was shaved and disinfected with alcohol and iodine. A sagittal incision was made along the midline of the skull and the periost was scraped to the sides using cotton swabs and scalpel. Lambda and

bregma (Figure 4) were used as reference points to align the skull to the horizontal plane. The sagittal sinus was revealed by thinning the bone along the midline of the skull in order to find the exact midline of the brain. Sagittal sinus, together with the transverse sinus, lambda and bregma served as reference points to calculate injection coordinates.

Viral tracers were injected in the dorsomedial medial entorhinal cortex in the right hemisphere with a Hamilton syringe (Hamilton Company, USA). The stereotaxic coordinates for all injections were 0.20 *mm* posterior to the transverse sinus, 3.00 *mm* lateral to the sagittal sinus and 1.90-2.00 *mm* deep from the dura mater. After the needle had been lowered to the injection site it was left for 2 minutes to let the tissue settle around it. The virus was injected over a period of 10-15 minutes depending on the volume of the injection. After the injection the syringe was kept in place for 10 minutes to minimize leakage of virus into other brain areas along the needle tract. More information about specific injections is found in paragraphs 2.2.1 and 2.3.1.

After completion of the injections, the skin and skull were cleaned with a saline solution. The skin was sutured, followed by application of iodide on the skin to disinfect the area. Once the mouthpiece was removed, Rimadyl was injected and the animal was placed in a heating chamber to recover. When the animal was awake, it was put back in its cage, and observed the days following post-surgery. For a step-wise walkthrough of the surgery protocol and equipment used, see Appendix III.

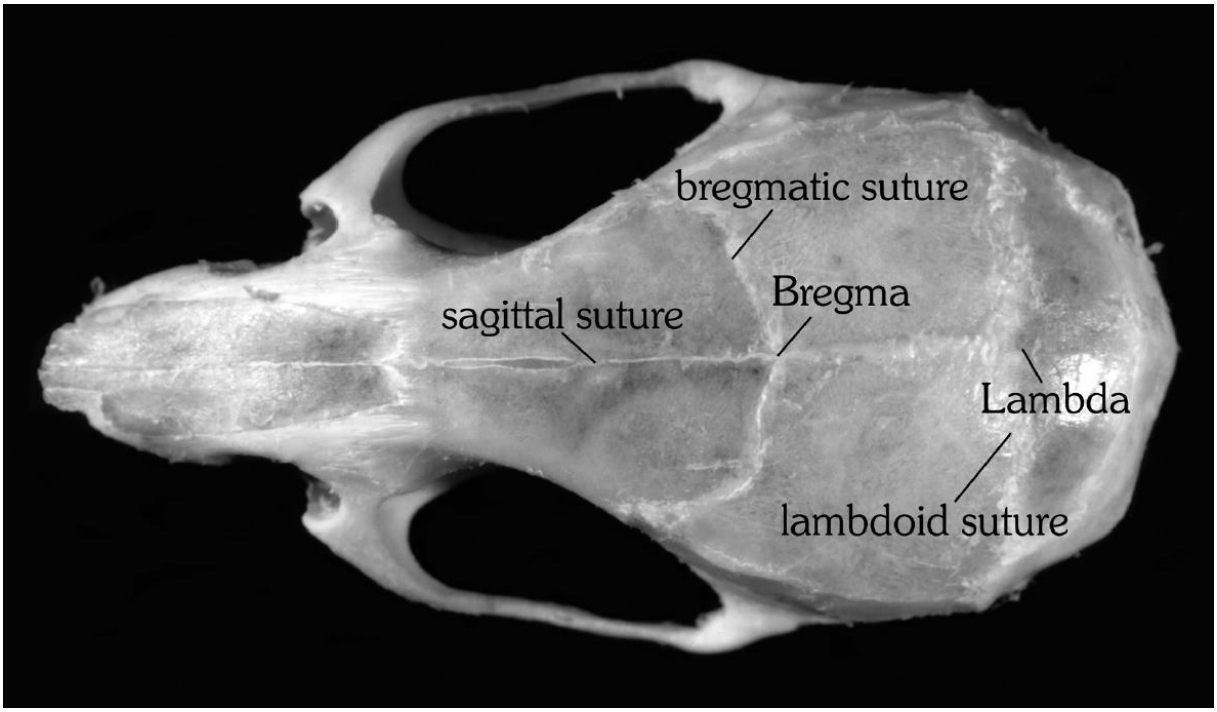

Figure 4. **Horizontal view illustrating the dorsal surface of a mouse skull.** Bregma and lambda are the nodal points where the bone plates of the mouse skull adjoin. Adapted from Franklin and Paxinos (2007).

2.1.4 Perfusion

At the end of each experiment the animals were weighed and deeply anesthetized with isoflurane before being euthanized with an intraperitoneal overdose of pentobarbital (Sanofi Sante, Maassluis, The Netherlands, 100mg/ml, 30-90mg/kg). Once all reflexes were absent, the animal was transcardially perfused. The animal's chest cavity was opened with scissors to expose the heart. A needle (27 gauge), connected to a peristaltic pump (World Precision Instruments Inc., USA) was inserted into the animal's left ventricle and the right atrium was cut open. A Ringer's solution (145mM NaCl, 3mM KCl, 2mM NaHCO3, pH 6.9) was pumped through the circulatory system until all blood had been removed, this was followed by day fresh 4% paraformaldehyde (PFA, Merck Millipore) in 0.125M phosphate buffer (PB) When the tissue was properly fixed, the brain was carefully removed from the skull and post-fixed in 4% PFA overnight at 4°C before being transferred to a solution containing 2% dimethyl sulfoxide (PB, 2% DMSO and 20% glycerol) for cryoprotection. The tissue was kept at 4°C until cutting.

2.1.5 Sectioning

The brains were sectioned on a freezing microtome (Microm HM430, Thermo Scientific, USA) and mounted with the ventral side down on the freezing stage with a PB solution containing

30% sucrose. The freezing stage was kept at - 30-35°C and dry ice was put on the brains to keep them frozen throughout the sectioning. All brains were cut in 40 µm thick horizontal sections from dorsal to ventral. Each brain was collected in 4 series, the first of which was immediately mounted on Superfrost Plus microscope slides (Gerhard Menzel GmbH, Braunschweig, Germany) with Tris-HCl. Remaining series were put in a cryoprotective medium and stored at -20°C for later use.

2.1.6 Nissl stain

Series that underwent immediate mounting were stained with Cresyl Violet (Sigma-Aldrich, St. Louis, USA) in order to accurately delineate cytoarchitectonic borders. Mounted sections were dehydrated with graded baths of ethanol, before 2 minutes of clearing in xylene. The sections were rehydrated, followed by a 2-4 minutes long bath in Cresyl Violet. The incubation duration varied with the age of the solution and the tissue quality, and due to this the sections were continuously monitored during the staining procedure. Excess Cresyl Violet was washed away by alternating between running water and 70% ethanol containing acetic acid. If the sections were lightly stained the above protocol was repeated until the sections were sufficiently dark. Finally, the sections were dehydrated and cleared in xylene, before being coverslipped with a mixture of xylene and entellan as the mounting medium.

2.1.7 Image acqusition and general data analysis

Immunostained brain sections were scanned in a digital slide scanner with a fluorescent lamp (Carl Zeiss, Jena, Germany, model Mirax Midi BF/FL v 1.12,) rigged with an Axiocam digital camera (Carl Zeiss, Jena, Germany), and filter sets 38 (BP 470/40) and 43 (BP 545/25) (Carl Zeiss, Jena, Germany) were used to obtain images of the different fluorophores used in the immunostaining.

High quality images of regions of interest were obtained with a Zeiss Meta 510 confocal microscope (Zeiss Imager.Z1, Jena, Germany) with Plan-Apochromat 10x/0.45 NA air, 20x/0.8 NA air and 40x/1.3 NA OiL DIC objectives. AF488 was imaged with the 488 laser line of an argon laser (dichroic mirror 488nm, emission BP filter 505-550nm) and AF546 with a helium-neon laser (dichroic mirror 561nm, emission BP filter 575-615IR)

To find the desired place for image capturing with the confocal microscope, each section was first overviewed with either 10x or 20x magnifying objectives. After a region of interest had been located, the tissue was scanned with 40x oil objective in Z-stacks to obtain high-resolution pictures of the cells somata. Clearly labelled cells with nicely stained somata were selected for confocal imaging. For simplification, the data analysis for the two main parts of the project will be described individually (Section 2.2.3 and 2.3.3).

Images used in figures had their contrast enhanced in Adobe Photoshop CS6 (Adobe Systems, San Jose, California, USA) to better visualize labelled cells compared to the background. Adobe Illustrator CS6 Extended (Adobe Systems, San Jose, California, USA) was used to create figures.

For delineation, Cresyl Violet stained tiled images were obtained from Neurolucida (MBF Bioscience, Williston, Vermont, USA). Tiled images (5x magnification) were obtained from each section with area of interest. The size and location of area of interest depend on labelled cells. See section 2.4 "Delineation of monosynaptic input structures" for more information about delineation.

2.2 Specificity of SST mouse line and distribution of somatostatin in the entorhinal cortex

2.2.1 Viral tracers and injection

A Cre-dependent reporter virus, AAV9-CAG-FLEX-GFP, was injected into the MEC (surgical procedure and injection coordinates are specified in paragraph 2.1.3) of a single SST-Cre animal. A total of 1µL of virus was injected over a period of 15minutes. Following the injection the needle was kept at the injection site for 10 minutes to ensure minimal spread of virus along the needle tract into other brain areas. A detailed description of the procedure is outlined in section 2.1.3 and Appendix III.

2.2.2 Immunohistochemistry

In order to display the distribution of SST expressing cell in the MEC, and to evaluate the specificity of Cre-expression in the chosen mouse line, immunohistochemistry (IHC) against the neuropeptide SST was performed. Subsequently, the overlap between cells expressing viral

GFP and labelled SST cells was counted and the total distribution of SST was evaluated. Overview of IHC protocols can be found in Appendix IV, solutions in Appendix V and list of chemicals in Appendix VI.

IHC protocol for Somatostatin

Sections were washed in 0.125 M PB for 3 x 15 minutes at room temperature, followed by an antigen retrieval step where the tissue was heat-treated for 2 hr at 60°C in 0.125 M PB. After this, the sections were washed in 0.125 M PB containing 1% Triton X-100 (PBT) for 2 x 10 minutes at room temperature to permeabilize the tissue. Following this step the sections were pre-incubated in a blocking solution of PBT containing 10% donkey serum at room temperature for 3hrs. The sections were then incubated for 48 hr at 4°C with the primary antibody against SST in PBT containing 10% donkey serum (1:500, goat polyclonal anti-SST, Santa Cruz Biotechnology). Following the incubation with the primary antibody the sections were washed in PB for 4 x 15 minutes before being incubated with the secondary antibody conjugated to the fluorescent marker; Alexa Fluor 546 (1:400, IgG donkey anti-goat AF546, Invitrogen) for 24 hr at 4°C. Finally, the sections were washed in PB (3 x 15 minutes) and Tris adjusted to pH 7.6 with HCl (Tris-HCl) (1 x 15 minutes) and subsequently mounted with Tris-HCl on SuperFrost plus microscope slides (Gerhard/menzel GmbH, Braunscweig, Germany) and air-dried overnight on a heating plate at 37°C. The following day the slides were coverslipped with a mixture of toluene and entellan.

2.2.3 Image acquisition and data analysis

Cell counting for the specificity of the mouse line and characterization of the SST cell population was done in confocal images. Microsoft Excel 2013 (Microsoft, Redmond, Washington, USA) was used to list all counted cells in a table and to make graphs. Adobe Illustrator CS6 and Adobe Photoshop CS6 Extended were used to make figures.

Regarding cell counting for the mouse line specificity, individual confocal images (40x oil magnification, Z-stack, 1x1 tiles) were taken throughout all sections with virally labelled GFP cells. The size of the Z-stack was determined by the most superficial labelled GFP cells in the tissue to the most deeply labelled GFP cells in the tissue. To get a representative selection of cells, images with high density of GFP cells and low density of GFP cells were selected. The confocal images were exported to Adobe Photoshop CS6 Extended and ZEN 2 (blue edition) (Carl Zeiss, Jena, Germany). ZEN 2 was used to go through the Z-stack and ensure that

overlapping GFP cells were counted individually. The overlap between GFP and SST labelled cells, and single labelled GFP cells were marked in Adobe Photoshop and quantified in Microsoft Excel.

Regarding cell counting for the distribution of the SST cell population, three tiled confocal images (40x oil magnification, Z-stack, 5x5 tiles) were taken. The images were selected as the most dorsal section in the dorsoventral axis of the MEC, an intermediate section in the dorsoventral axis of the MEC and the most ventral section in the dorsoventral axis of the MEC. The confocal images were exported to Adobe Photoshop and SST labelled cells were marked. Microsoft Excel was used to quantify SST cells. The counted sections were normalized to area size in Adobe Acrobat XI Pro (Adobe Systems, San Jose, California, USA). An image of the MEC sections were exported to Adobe Acrobat and the size of the region (superficial or deep layers) was traced with the “area tool” found in “measuring tools” in the tool section. The amount of cells was normalized to the size of the region.

2.2.4 Summary of the procedure used in 2.2

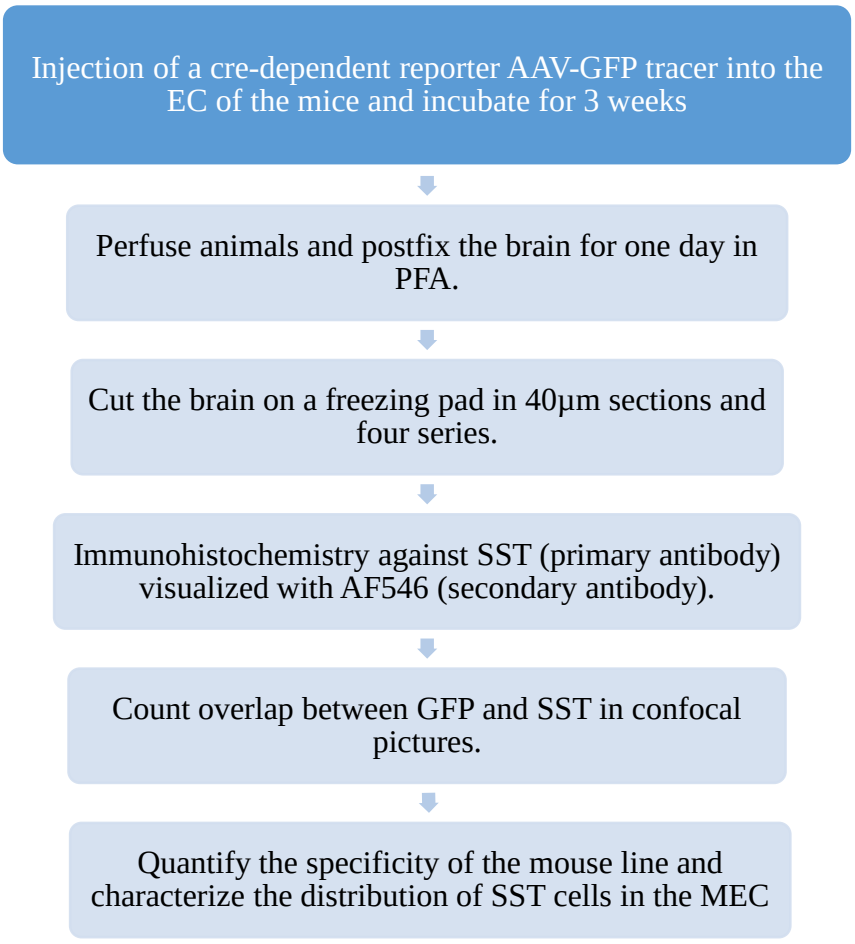

Figure 5. **Methods summary.** The procedure used to determine the specificity of the mouse line and the distribution of SST cells in the MEC. For abbreviations, see list of abbreviations.

2.3 Monosynaptic tracing experiments

2.3.1 Viral tracers and injection

Four different injection strategies have been used for the monosynaptic experiments. Two different types of virus were used, a helper virus that infects SST-cells expressing Cre, and a rabies virus specific for the helper virus. In all animals the injections were done as follows; one minute waiting time before injecting the virus; one bout of virus injected each minute for a time period of 10 minutes; and at last, wait for 10 minutes before removing the needle from the tissue. The viruses used were in-house made by Rajeevkumar R. Nair, PhD. Coordinates for injections are found in paragraph 2.1.3, whereas details about animals can be found in Appendix I.

The first round of injections was done with an AAV helper virus expressing GFP in Cre-positive cells and an EnvA-pseudotyped G-deleted rabies virus expressing mCherry. 200-300 nL of AAV virus was injected at the specified coordinates, followed by three weeks of incubation. 500 nL rabies virus was injected at the same coordinates, followed by seven days of incubation before the animals were terminated. The second and third injection strategies were done with mixed injections of AAV and rabies virus in the same needle. Two parts AAV and three parts rabies to a total of 600 nL were injected in the second strategy, followed by an 8 days incubation period. In the third strategy, AAV and rabies was mixed to an equal amount and injected at a total of 1 µL, followed by a two week incubation period. For the fourth injection strategy, separated injections were used. 400 nL of AAV virus was injected into the MEC. After two weeks of incubation, 500 nL of rabies virus was injected, followed by another incubation period of two weeks. Details about viral strategies are given in Appendix II, table 4

2.3.2 Immunohistochemistry

To amplify the products of the viral expression in the MEC, immunohistochemistry was performed against the fluorescent proteins GFP and mCherry, as well as against the small protein tag, influenza hemagglutinin (HA).

IHC protocol for Green Fluorescent Protein and mCherry

The same immunohistochemistry protocol was used for the fluorescent proteins GFP and mCherry. The sections were washed in 0.125M PB for 4 x 15 min at room temperature, followed by an incubation in primary antibody for 48 hr at 4C°, the incubation solution consisted of PBT with 0.5% DMS, 1% natural goat serum (NGS) and primary antibody against mCherry (1:500, IgG mouse anti-mCherry, ClonTech) and GFP (1:500, IgG rabbit anti-GFP, Life Technologies). After the incubation, sections were washed in PB for 6 x 15 min at room temperature. The sections were then incubated with a secondary antibody conjugated with fluorescent marker AF488 (1:500, IgG α-rabbit AF488, Invitrogen) for GFP and AF546 (1:500, IgG α-mouse AF546, Invitrogen) for mCherry, the same incubation buffer as above was used. The following day, the sections were washed with PB for 5 x 15 min and in Tris-HCl 15 min, mounted and air-dried overnight. At last, the slides were coverslipped.

IHC protocol for HA tag

The sections were washed at room temperature in PBT for 4 x 15 minutes, followed by another wash for 3 x 10 min in Tris with pH 8.0. To enhance permeabilization, the sections were washed for 2 x 10 min in Tris + 0.5% Triton x-100 (Trx), before incubation with primary antibody against the HAtag (1:100, rat α-HA,) for 4 days at 4°C. Subsequently, the sections were washed 4 x 15 minutes in Tris-HCl pH 8.0 at room temperature, and after this incubated in secondary antibody goat anti-rat Alexa Fluor 546 (1:400, IgG goat α-rat AF546, Invitrogen) in Tris + 0.5% Trx for 24 hr at 4°C. The next day, the sections were mounted and dried on a heating place at 37°C overnight before they were coverslipped.

2.3.3 Image acquisition and data analysis

Cell counting of monosynaptic inputs to the MEC was done with Neurolucida, MIRAX images and in confocal images. Microsoft Excel was used to list all counted cells in tables and to make graphs. Adobe Illustrator CS6 and Adobe Photoshop was used to make figures.

Neurolucida's meander scan 10x magnification was used to count each individual section in brains with positive monosynaptic transport of rabies virus. Tracing from each individual section was superimposed onto images of Cresyl Violet staining and regions with positive cells were delineated based on cytoarchitectonical features (Described in 2.5). MIRAX images were used to get an overview of sections with positive cells and to double check cells previously counted in Neurolucida. Confocal images (40x oil magnification, Z-stack, 1x1 tile) were taken from rabies virus labelled cells to be used in figures.

To characterize the starter cell population, confocal images were obtained from all the sections with positively rabies virus labelled cells situated around the injection site. The overlap between rabies virus labelled cells (GFP or mCherry) and AAV labelled cells (GFP or HA-tag conjugated with AF546 or 488) was quantified.

2.3.4 Summary of the procedure used in 2.3

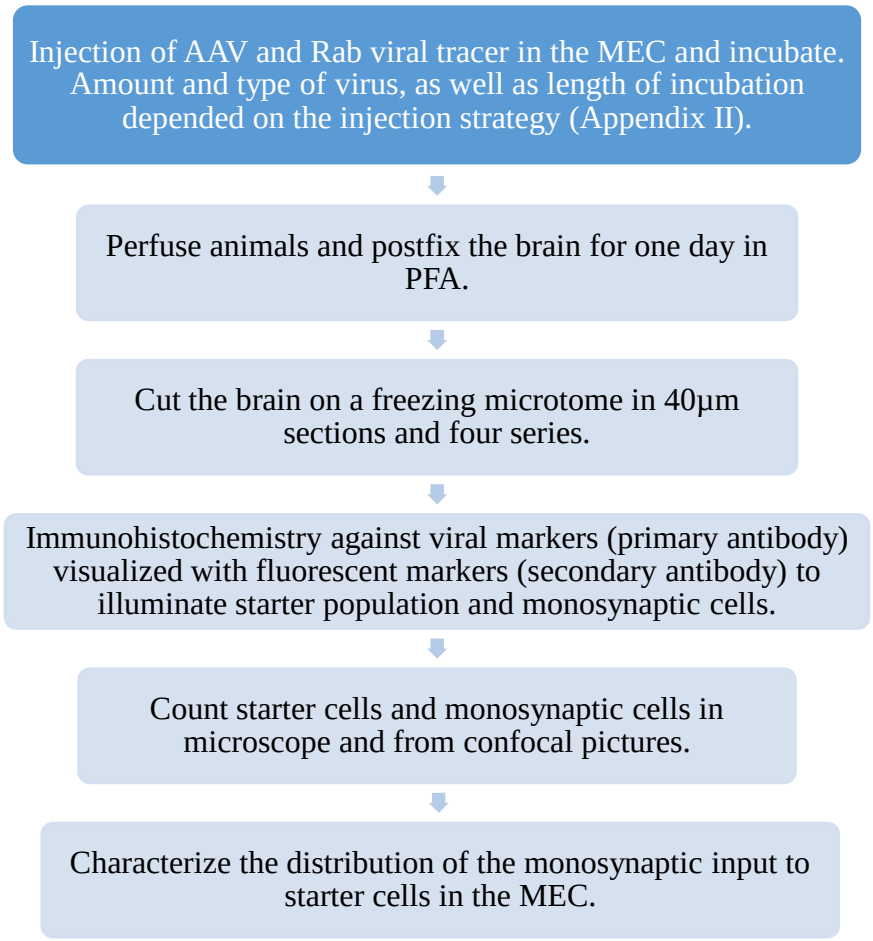

Figure 6. **Methods summary.** The procedure used to characterize the monosynaptic input and starter cell population of the MEC. For abbreviations, see list of abbreviations.

2.4 Delineation of monosynaptic input targets

Delineations of brain regions were done in horizontal sections stained with Cresyl Violet from the mouse brain with monosynaptic transport of virus. Rough delineations of areas were done according to a stereotactical atlas (Franklin & Paxinos 2007), but in order to precisely describe the borders between structures and laminar organization within structures, previously described cytoarchitectonical hallmarks for them were considered. Only structures with viral transport were selected to be delineated. Hence, many regions in the HF and the PHR are not described.

2.4.1 Delineation of the HF

The subregions of the Cornu Ammonis

The CA consists of three subfields, the CA3, the CA2 and the CA1, each having their own set of characteristics (Boccara et al. 2015; Cappaert et al. 2015). As described in the literature, all CA fields have the same general laminar organization in the HF. The most prominent layer is the stratum pyramidale, a clearly visible layer with densely packed principal cells. The stratum oriens, a narrow polymorphic almost cell-free layer that lies deep to the pyramidal layer. Superficially to the stratum pyramidale sits the stratum radiatum, and most superficially the stratum lacunosum moleculare (Freund & Buzsáki 1996; Boccara et al. 2015; Cappaert et al. 2015), The CA3 is characterized by large, densely packed pyramidal cells, as well as the stratum lucidum a thin lightly stained layer wedged between stratum pyramidale and stratum radiatum. Stratum lucidum is only found in this region and is characterized by the almost complete absence of neurons. CA3 distal border is to the DG, while proximally it borders the CA2. Identifying the border of CA3 with the CA2 was difficult in Cresyl Violet stains as it was not clearly demarcated. However, a visible hallmark was a slight, abrupt widening of the pyramidal cell layer (Boccara et al. 2015). This was accompanied by a decrease in pyramidal cell size, as well as the cell layer being loosely packed. As the CA2 bordered the CA1, its cell population contained a mixture of large and small pyramidal cells (Cappaert et al. 2015). The CA1 was most easily recognized by its striking homogeneous pyramidal neurons that arrange the stratum pyramidale into a neat lamina (Figure 7). In stained sections the deeper part of the CA1 pyramidal layer seemed to be more loosely arranged than its superficial part. Distally, the CA1 borders the subiculum (Boccara et al. 2015; Cappaert et al. 2015). Identifying this border was done by looking for a sudden increase in the width of the stratum pyramidale from a thin layer in the CA1 to a wider less organized layer in the subiculum (Boccara et al. 2015).

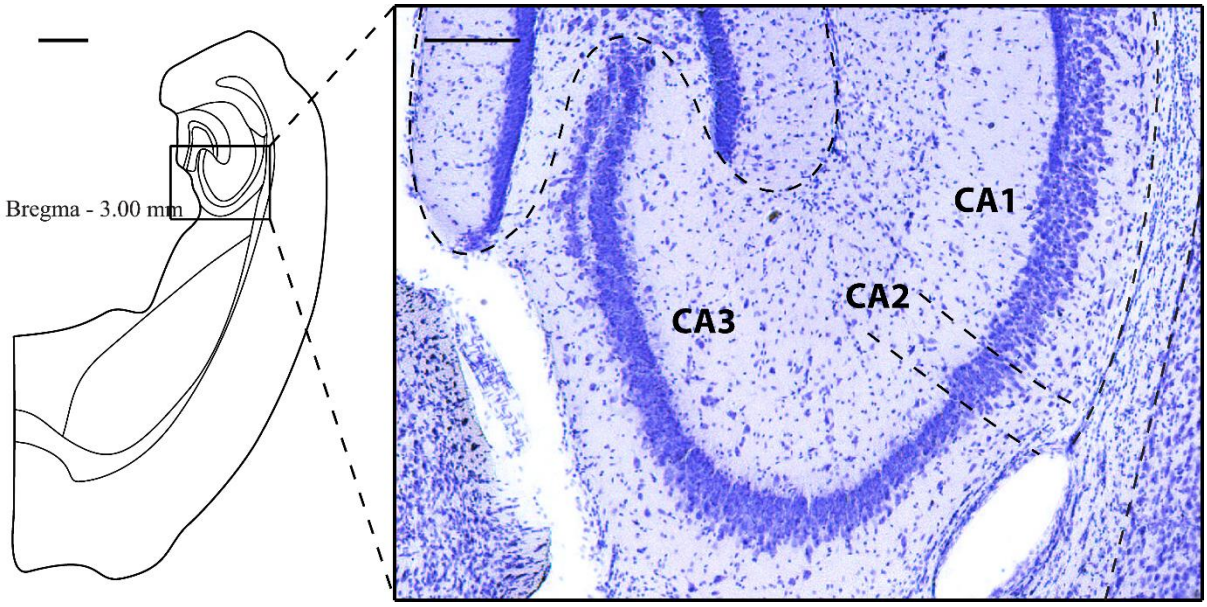

Figure 7. **Intermediate section of the CA subregions in the hippocampal formation.** Border with the DG, between CA subregions and the alveus are indicated by dotted lines. The CA3 has a darkly stained, densely packed pyramidal cell layer. The CA2 with a slightly wider pyramidal cell layer with cells of mixed size, and the CA1 with a loosely organized pyramidal cell layer. Scale bars for overview 1mm; delineation 200µm. For abbreviations, see list of abbreviations.

2.4.2 Delineation of the PHR

The Presubiculum

The PrS was treated as one structure without further subdivisions. As a structure in the PHR, the PrS has six layers (Boccara et al. 2015). The superficial layers, LII and LIII are characterized by their small, dark, densely packed cells, with LIII being distinguished from LII by its looser arrangement of cells. Due to the characteristic cells sparseness of the lamina dissecans, it was clearly visible as it divides superficial layers LII/III from deep layers LV/VI (Boccara et al. 2015; Cappaert et al. 2015). The PrS borders the subiculum medially, the border was differentiated by looking at the size of cells, as subicular cells are larger and more loosely arranged compared to PrS cells (Figure 8). The distal border of the PrS to the PaS could be difficult to differentiate. However, the superficial layers could be told apart by looking at cell size as the cells in the PaS were large and LII and III more continuous than in the PrS (Boccara et al. 2015; Cappaert et al. 2015). As deep layers could not easily be separated I chose to place the border radially to the cortical surface at the LII/III border between the PrS and PaS. Dorsally, the PrS borders the RSC. A hallmark characteristic of this border was the absence of

the lamina dissecans in the RSC (Boccara et al. 2015), this was the feature I used to separate the two areas from each other.

The Parasubiculum

The cytoarchitectonics of the PaS were very similar to those of PrS. Like other structures of the PHR the PaS has six layers, layers II/III contain large, densely packed, lightly stained pyramidal cells, and contrary to the observable lamination of superficial layers in the PrS and the MEC, LII and III could not be distinguished from each other in the PaS (Boccara et al. 2015; Cappaert et al. 2015). This was one of the defining features used to tell the PaS apart from its neighbouring regions, figure 8. A pronounced cell sparse lamina dissecans divided the superficial layers from deeper layers, similar to the neighbouring regions the PrS and the MEC (Boccara et al. 2015). It should be noted that to delineate the deeper layers of the PaS from neighbouring regions in Cresyl Violet stained sections was difficult (Boccara et al. 2015).

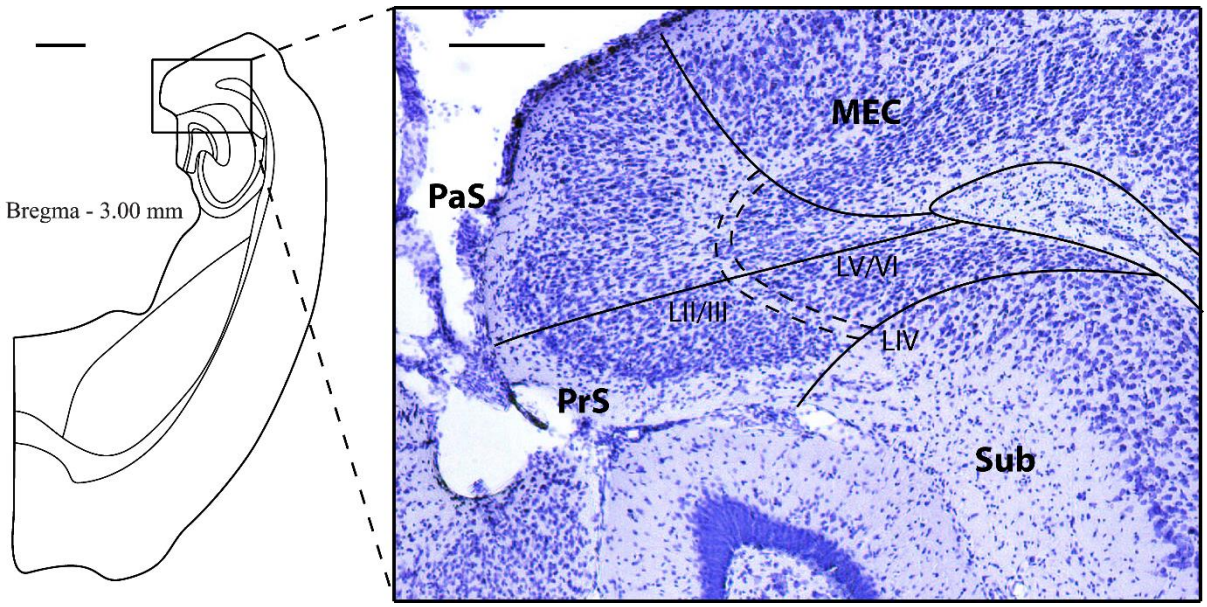

Figure 8**. Intermediate section of the presubiculum and parasubiculum delineated.** Border between the parasubiculum and the presubiculum and to the medial entorhinal cortex and subiculum can be seen illustrated with black lines. Lamina dissecans indicated by dotted lines. Deeper layers V/VI separated from superficial LII/III by LIV, lamina dissecans. For abbreviations, see list of abbreviations.

The Medial Entorhinal Cortex

The MEC was considered as one structure without taking its subdivisions (Insausti et al. 1997; Boccara et al. 2015) into account when delineating the brains. As described by Ramon y Cajal the MEC could be seen as a six layered structure at the ventrocaudal end of the rodent brain

(Cappaert et al. 2015). Hallmarks of the MEC architecture were the large darkly stained cells packed together in LII and the clear transition into a more uniform LIII with intermediately sized pyramidal looking cells (Boccara et al. 2015). The lamina dissecans or LIV was very clearly visible in horizontal sections, and L V/VI could be recognized by medium to small pyramidal cells that were organized in radial columns (Insausti et al. 1997) – a feature which distinguished the MEC from its neighbouring structures, figure 9. The MEC borders the PaS medially (Boccara et al. 2015; Cappaert et al. 2015). The border was recognized by looking at the organization of LII/III where the MEC had a marked transition between these two layers, which the PaS lacks (Boccara et al. 2015). The lamina dissecans in certain cases also seemed more pronounced in the MEC than in the PaS. Dorso-laterally, the MEC is bordered by the POR (Boccara et al. 2015; Cappaert et al. 2015). Identifying the dorsal border with the POR could be difficult, however the POR and the MEC can be told apart by looking at the construction of LII, where LII in the POR had a more irregular appearance than that of the MEC, as well as a disappearing lamina dissecans. Neurons in LII of the POR are also smaller than in LII of the MEC (Boccara et al. 2015). Ventrally, the LEC occupied the lateral border of the MEC. This border could be recognized mainly by two key features. Firstly, LII changed its appearance from homogenously arranged cells in the MEC to islands of large cells in the LEC, and in certain parts of the LEC LII also appeared to be divided in two cell zones. Secondly, the LEC had a less clearly defined lamina dissecans that functioned as a good landmark for separating the two areas (Cappaert et al. 2015).

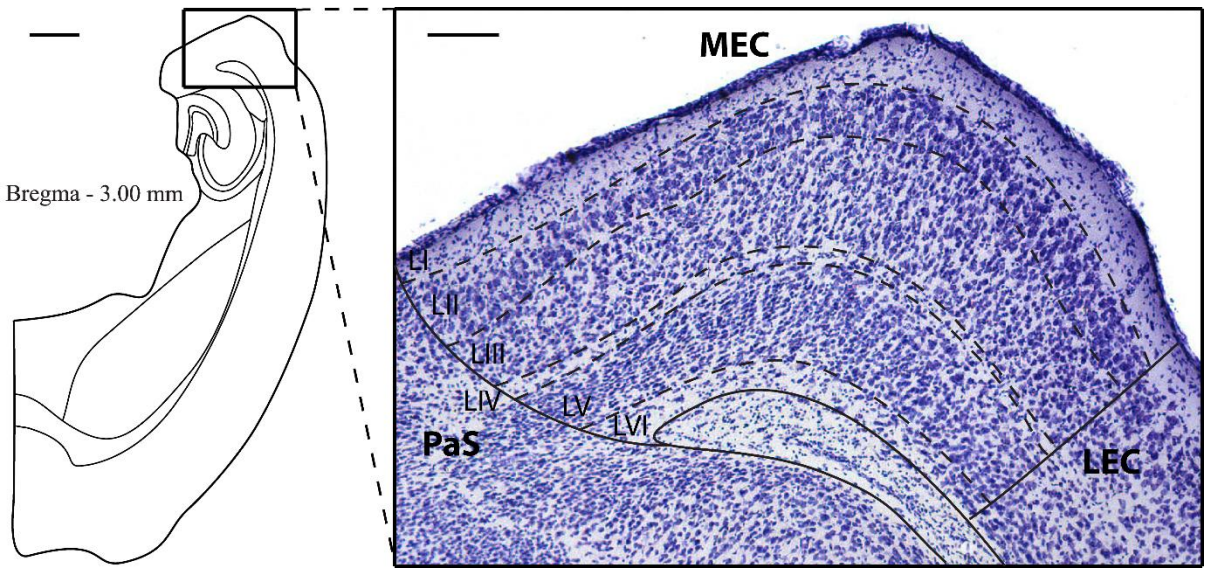

Figure 9. **Intermediate sections of the medial entorhinal cortex delineated.** Border with the parasubiculum and postrhinal cortex can be seen illustrated with black lines. Laminae indicated by

dotted lines. LII with darkly stained large cells. LIII with loosely organized medium sized cells. LV/VI with radially stacked columns of cells. Scale bars overview 1mm; delineation 200µm. See list of abbreviations.

2.4.3 Delineation of neocortical structures

The Retrosplenial cortex

The RSC has been described to consist of multiple subdivisions (Vogt & Paxinos 2014). However, I will only consider the cytoarchitectonics for area 29a since it is the most ventral subdivision of the RSC, and the area where I observed labeled cells (Vogt & Vogt 2004). The structure is located in the dorso-caudal regions of the mouse brain, where its ventral portion borders the dorsal subregions of the HF and PRH (Cappaert et al. 2015). The general six-layer laminar organization was seen. Superficial layers were composed of a narrow LII with small darkly stained cells and a slightly wider LIII/LIV, although LIV is hardly visible in Cresyl Violet stains. LV is a wider homogeneous lamina, containing larger, lightly stained cells. LVI is narrow and characterized by a drop in cell size compared to LV (Vogt & Vogt 2004). The RSC border to the dorsal PrS is characterized by slightly smaller cell bodies in the RSC and a disappearing lamina dissecans in the transition to the RSC (Vogt & Vogt 2004; Cappaert et al. 2015). Deep to layer VI, the RSC borders the HF. Identifying this border was done by looking for a sudden drop in cell density and homogeneity (Figure 10).

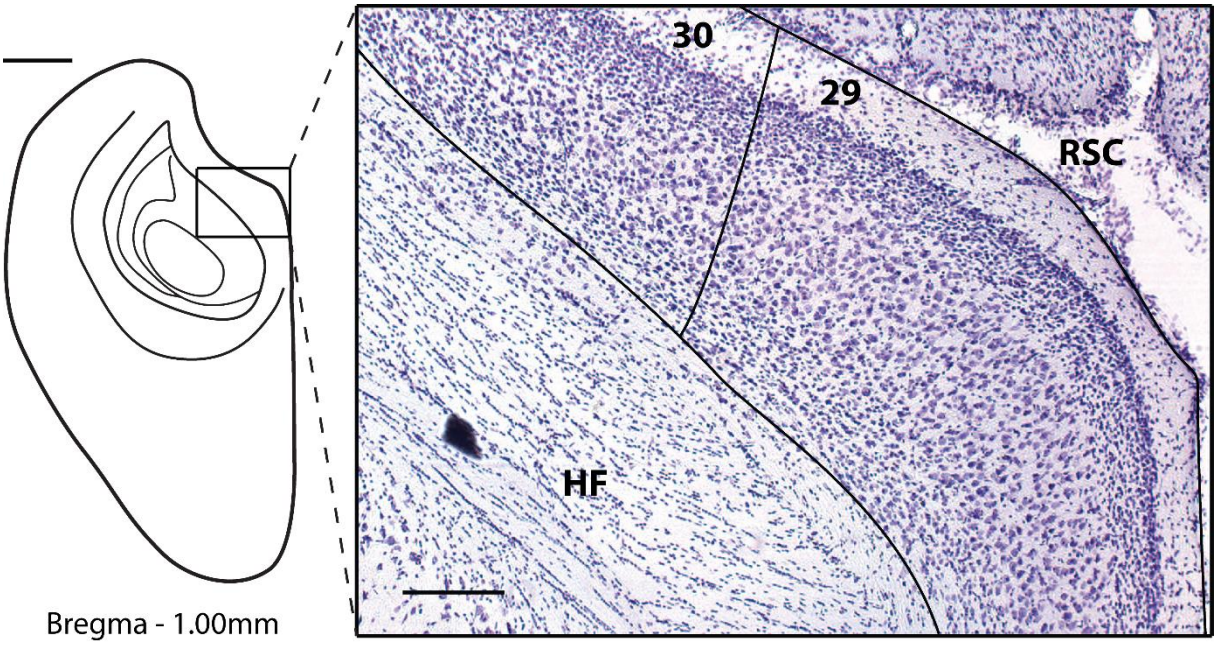

Figure 10. **Dorsal section of the ventral retrosplenial cortex delineated.** Border with the Area 30 and Area 29 of the RSC and the dorsal hippocampus can be seen indicated by black lines. Scale bars of overview 1mm; delineation 200µm. For abbreviations, see list of abbreviations.

2.4.4 Delineation of subocortical structures

The Medial Septum

The MS is a nucleus in the basal forebrain of rodents. It is a compound structure of cholinergic, glutamatergic and GABAergic projection neurons, but it also contains several subgroups of interneurons (Zaborszky et al. 2012). It cannot easily be delineated based on cytoarchitecture because the different cell types differ in size, orientation and location within the nucleus. Using several different staining techniques together is the best way to identify the borders of the MS. In my data a few cells were found centrally in the medial septal structure, thus, the Paxinos atlas of the mouse brain was the main tool used in order to identify the area. The cytoarchitecture of the area itself was compared to the atlas, and identification of surrounding structures also aided

the identification of the area. Figure 11 shows the approximate level where I found MS cells, the structure is marked with diffuse borders as they are not easily defined.

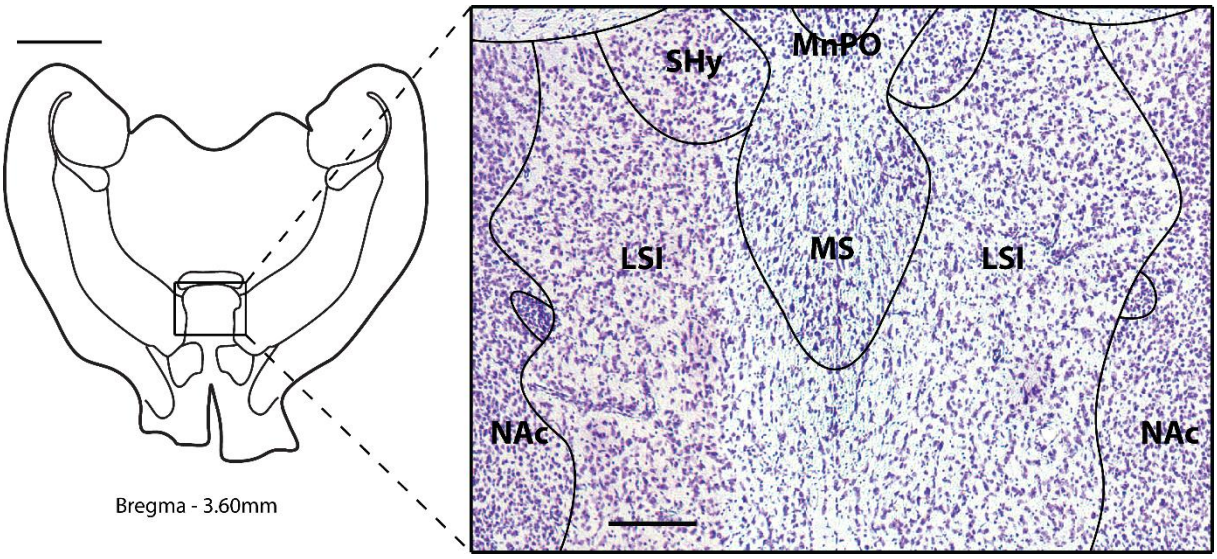

Figure 11. **Ventral section of the medial septum delineated.** Borders with the lateral septal nucleus (LSI), the septohypothalamic nucleus (Shy) and the Median Preoptic nucleus (MnPO) indicated by black lines. Scale bars overview 2mm; delineation 200µm. For abbreviations, see list of abbreviations.

Chapter 3 Results

3.1 Mouse line specificity and distribution of SST-positive cells in entorhinal cortex

3.1.1 Specificity of the SST-cre mouse line

Two animals were used to check the specificity of the transgene expression in our mouse line (Ssttm2.1(cre)Zjh/Jax). This part of the project was a collaboration with another master student in the lab (Gjermund K Jordheim). An AAV viral vector expressing GFP in the presence of cre-recombinase was injected into the animals to show transgene expressing cells. Immunohistochemistry against SST was conducted in order to estimate how many of the cre-expressing cells also expressed SST. Due to difficulties identifying immunopositive cells with normal florescence microscopy, confocal samples of the tissue were made in order to do the counts. The mouse line expressed the transgene with high specificity in both cases (82 and 84%), and there did not seem to be differences in the specificity across the dorsoventral axis (data not shown). Figure 12 shows the percentage of cells labelled with GFP (light green) and the number of cells labelled with both GFP and immunohistochemistry against SST (dark green) in the two individual animals. Figure 13 shows a representative image from the MEC with viral expression of GFP (green) and immunohistochemistry against SST (greyscale).

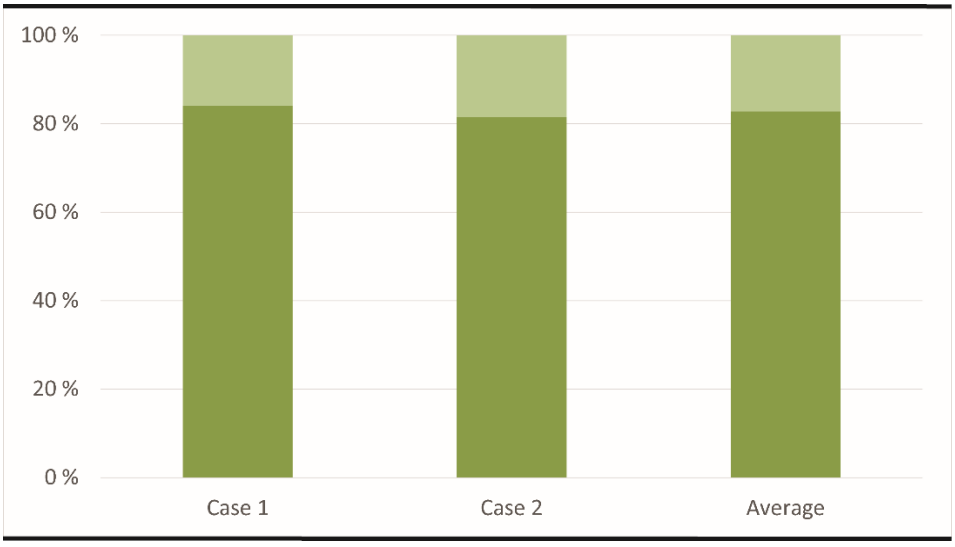

Figure 12. **The transgene expression of the mouse line is highly specific.** Stacked bar graphs showing the percentage of GFP expressing (light green) cells that stain positive for SST with immunohistochemistry (dark green). In Case 1 84% (n = 173/206) of the transgene expressing cells

show SST expression through IHC, and in Case 2 the overlap was 82% (n = 411/504). The average overlap was 83% (n = 584/710).

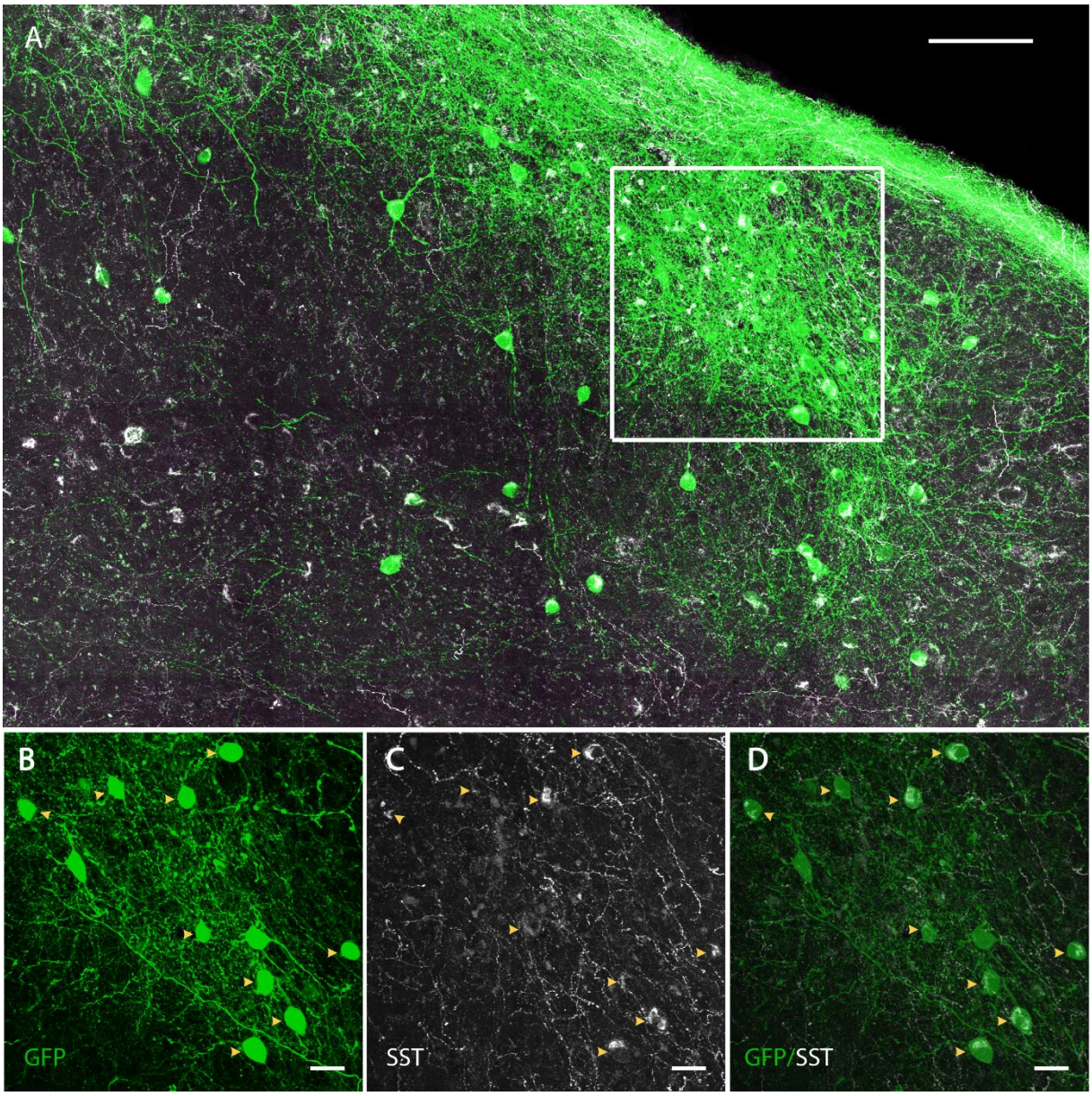

Figure 13. **Representative image of GFP expression and immunostaining against SST.** A) Overview image from a representative area used to count the overlap. B) GFP expression from virus C) Somatostatin cells labelled by IHC D) Overlap between the two populations of cells. Yellow arrows indicate cells with overlapping stains. Scale bars A) 100µm, B)-D) 20µm. For abbreviations, see list of abbreviations.

3.1.2 Distribution of somatostatin in the medial entorhinal cortex

Sections from one animal were used to characterize the distribution of SST cells in the MEC. The same animal had also been used to investigate the specificity of the mouse line (Case 1 in

section 3.1.1). The data in the analysis were based on cell counts from IHC against SST. Due to limited time, three sections were chosen to represent dorsal, intermediate and ventral regions of the MEC. Sections from the same animal, stained with Cresyl Violet were used to delineate each individual section. Figure 14. illustrates the three different sections where cells were counted, with corresponding confocal images of the SST IHC, and outlines of each area with individual cells marked by green circles.

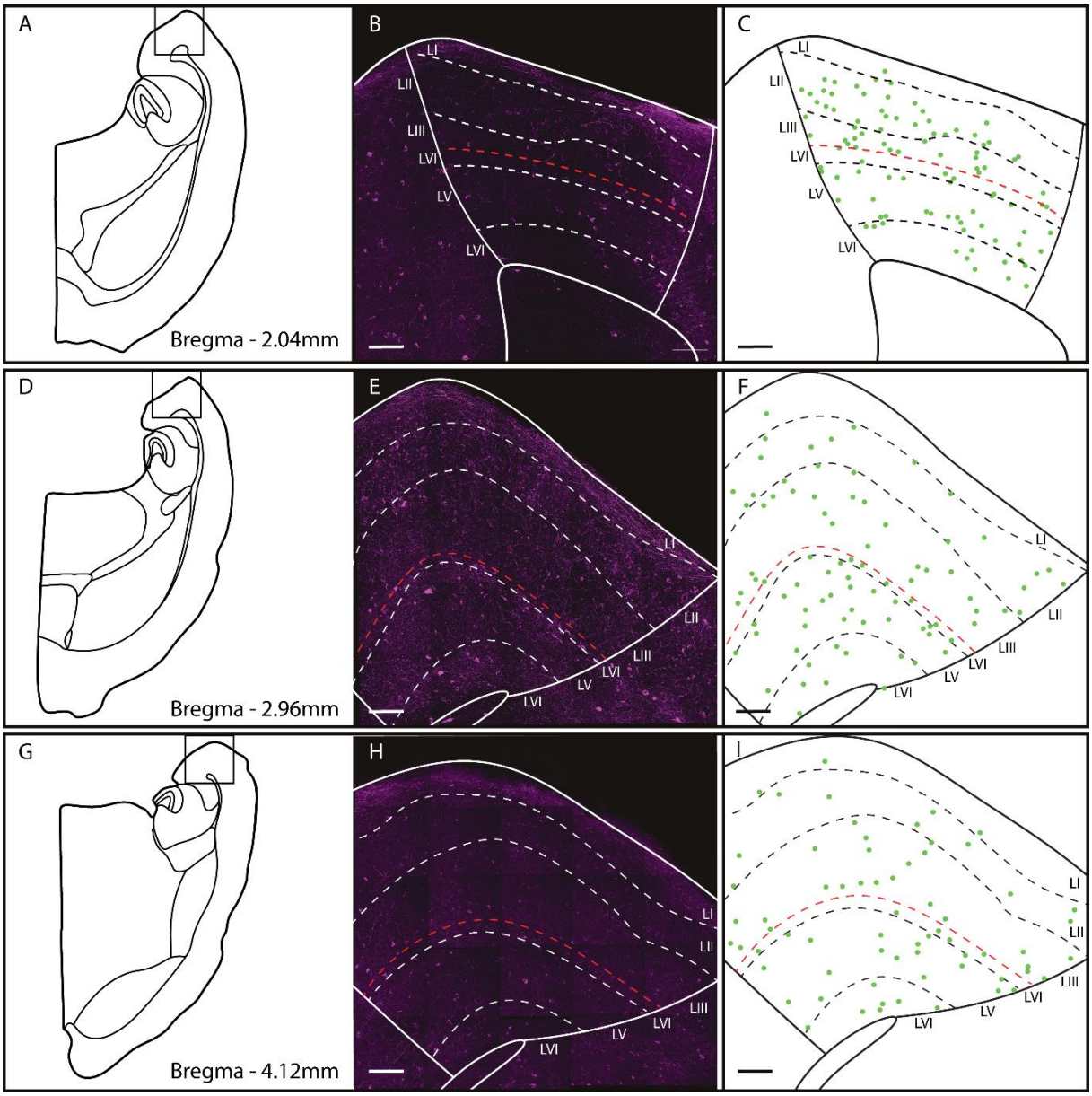

Figure 14. **Distribution of somatostatin cells across the MEC.** The left column shows outlines of the sections at different dorsoventral levels where cells were counted (A, D, G). The middle column shows the confocal images (40x, oil objective) used to count the SST positive cells (B, E, H). The right column **s**hows outlines of the counted areas with green dots indicating SST positive cells (C, F, I). The red line represents the border between superficial and deep layers. Scale bars represents 100µm.

The counts showed that there was a slight decrease in the number of SST positive cells from dorsal to ventral sections. Figure 15A shows the distribution of counted cells along the dorso-ventral axis. When considering the laminar distribution in individual sections, I noticed a tendency for more SST cells to be situated in superficial compared to deep layers. Superficial layers included LI to LIII, and deep layers included the lamina dissecans, LV and LVI. The red line in figure 14 represents the border between superficial and deep layers. The intermediate section did not show the same trend, and there did not seem to be any superficial to deep difference in this section (Figure 15, B).

As the laminae of the MEC vary in size, I decided to normalize the cell counts to the relative size of each area. This showed that more SST cells were found in deep layers compared to superficial layers in the intermediate and the ventral sections (Figure 15, C). The dorsal section did not show the same trend, and more or less equal counts pr. area were found in superficial and deep layers. Overall, the number of SST cells was larger in deeper layers compared to superficial layers when considering the size of the area counted (Figure 15, D).

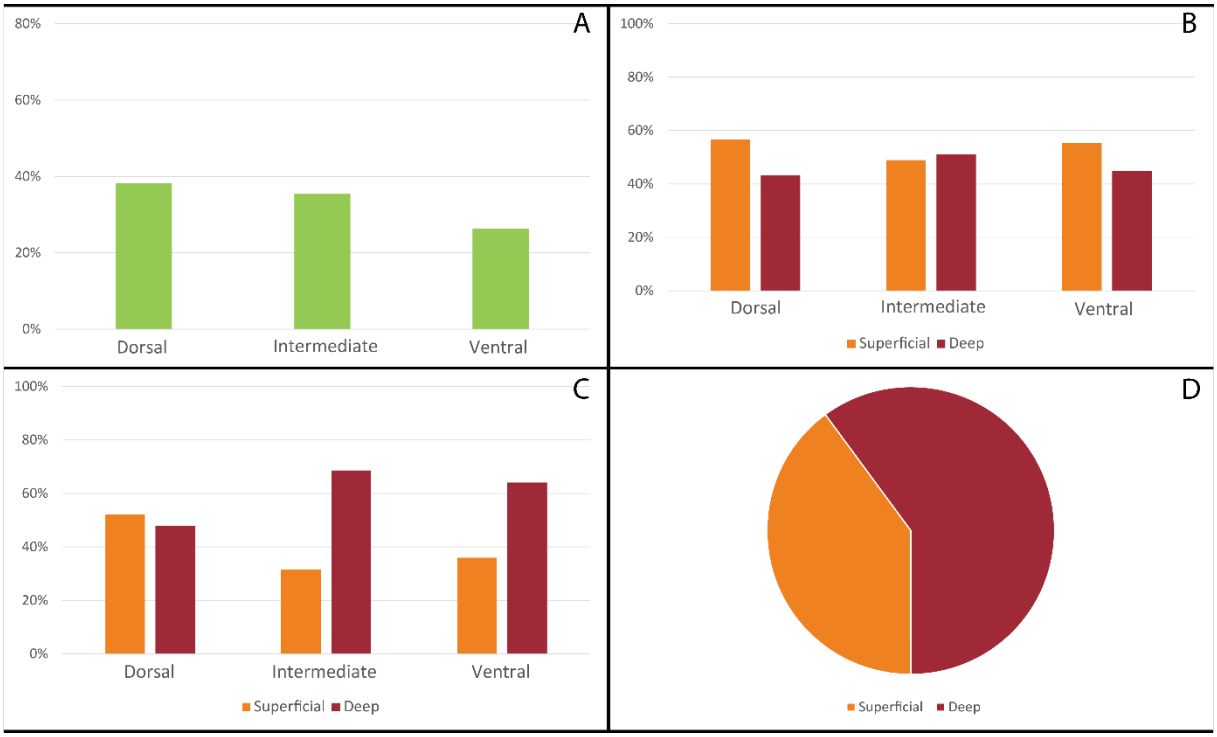

Figure 15. **Distribution of somatostatin positive cells in the medial entorhinal cortex.** A) Cells counted in individual sections of the MEC compared to the total amount of cells counted in the MEC (dorsal n = 97; intermediate n = 90; ventral n = 67). B) Distribution of cells in superficial and deep layers

throughout the dorso-ventral axis. C) Distribution of cells in superficial and deep layers throughout the dorso-ventral axis normalized to area size. D) Overall distribution of SST cells in superficial (n = 136) and deep (n = 118) layers normalized to area size.

3.2 Strategies for tracing the monosynaptic inputs to SST cells in the MEC

As the viral tracing system used in this project was new in my hands, four different viral tracing strategies were tested in order to optimize the monosynaptic tracing protocol. My goal was to trace an adequate number of connections while confining the injection to the desired area.

3.2.1 Overview of viral strategies

Four different viral strategies were used in 18 animals, and two different areas of the brain. All the cases from injections to the MEC (Martin Øvsthus) and the LEC (Gjermund K Jordheim) are presented in table 1. The different strategies gave us various results, which is indicated by different colours; Green – good viral transport, indicates long-distance monosynaptic transport; Yellow – poor viral transport, indicate local viral transport; Red – no viral transport, and unusual expression written in orange. Asterisks indicate that the injection missed its designated area. Strategy 1 resulted in two cases with bad transport (#52941 and #52607), one with poor viral expression within the LEC (#52209) and one successful case with long-distance transport (#52211). Strategy 2 resulted in three cases with bad transport (#52605, #52604 and #52609) and one case with local starter cells and monosynaptic transport within the MEC (#52823). Strategy 3 resulted in three bad cases (#53588, out of place, #53048 and #53047), two with poor viral transport (#53586 and #53050) and two with good transport, but with injection out of place (#53051 and #52939). Strategy 4 resulted in two cases with good monosynaptic transport (#54793 and #54794), however, one was out of place. The last strategy also resulted in one case (#54799) with anterograde viral transport.

Table 1. **Overview of viral strategies used for labelling cells in the MEC and the LEC.** Green – Good viral transport with monosynaptic labelling outside the entorhinal cortex. Yellow – Poor viral transport within the EC. Red – no viral transport.

Viral strategies	*MEC*		*LEC*	
*Strategy 1***	52941	52211	52607	52209
*Strategy 2****	52823	52605	52604	52609
*Strategy 3****	53586	53588*	53051*	53048
	53047	-	53050	52939*
*Strategy 4***	54799	-	54793*	54794

Good viral transport	No viral transport	Poor viral transport	Unusual expression

* Injection out of place.
** Separated injections with AAV helper virus and rabies.
*** Mixed virus with AAV helper virus and Rabies injected in the same injection.

3.3 Monosynaptic inputs to the MEC

From 8 animals, only one case had long-distance transport of rabies virus. Three more animals had local transport of rabies virus, but no long-distance projections were found. The case with long-distance transport outside the MEC will be included in the paragraph about extrinsic connectivity, while cases with local transport within the MEC will be included in the paragraph about intrinsic connectivity.

3.3.1 Extrinsic connectivity of SST cells in the medial entorhinal cortex

One animal had sparse long-distance transport of rabies virus to structures outside the borders of the MEC. Inputs to SST cells in the MEC were found in the PHR and the HF as well as a few cells in the neocortex and in subcortical structures.

Starter cells

The starter cells were defined as cells that expressed both the tag from AAV helper virus (GFP) and the fluorescent protein from the rabies virus (mCherry). Thirty-one starter cells were found in the MEC of the one case with long-distance transport. The starter population was largely confined to dorsal regions of the MEC. Figure 16 A shows that the majority of starter cells was confined to deeper layers, LV and LVI, of the MEC. Starter cells were also identified in superficial layers, but in lower numbers. Additionally, starter cells were identified in structures bordering the dorsal MEC (Figure 16 B). A considerable number of starter cells were situated in what seemed to be a transition region between the MEC and the POR. However, the

cytoarchitecture of the area was difficult to recognize as there was considerable gliosis and tissue damage in the area from the tract of the injection needle. The cytoarchitecture on the contralateral side was clearly MEC-like. However, it seemed the brain had been cut with a slight tilt, and it is thus possible that some of the starter cells were located in the POR. I therefore, chose to represent these cells in a separate category in the results for clarification (Figure 16 B).

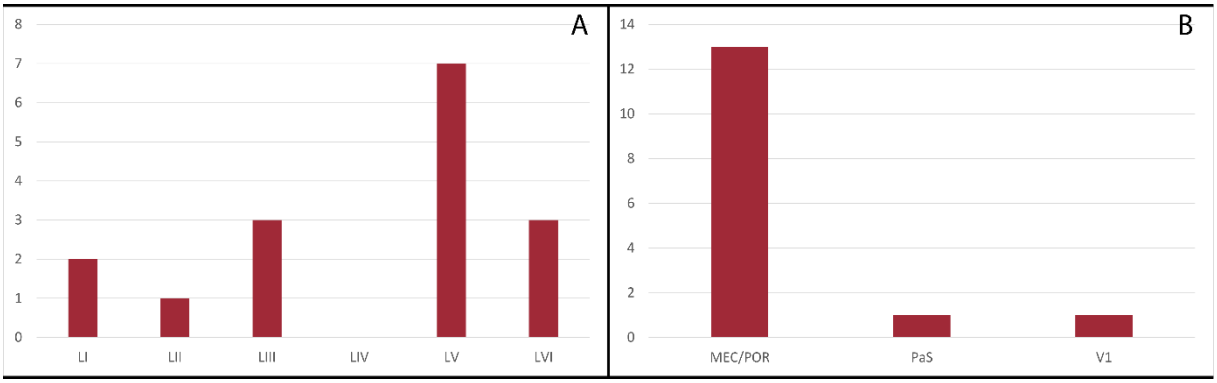

Figure 16. **Distribution of starter cells.** A) Shows the layered distribution of starter cells found within the MEC. B) Shows starter cells found outside of the MEC and at the MEC border. For abbreviations, see list of abbreviations.

Monosynaptic inputs from the PHR

Monosynaptically mCherry labelled cells were found in a few locations throughout the PHR. Figure 17 shows the distribution of monosynaptically labelled cells in the PHR, apart from the MEC. A total of seven labelled cells were identified. Four of these were seen in the PrS, two in the PaS and one in the PER.

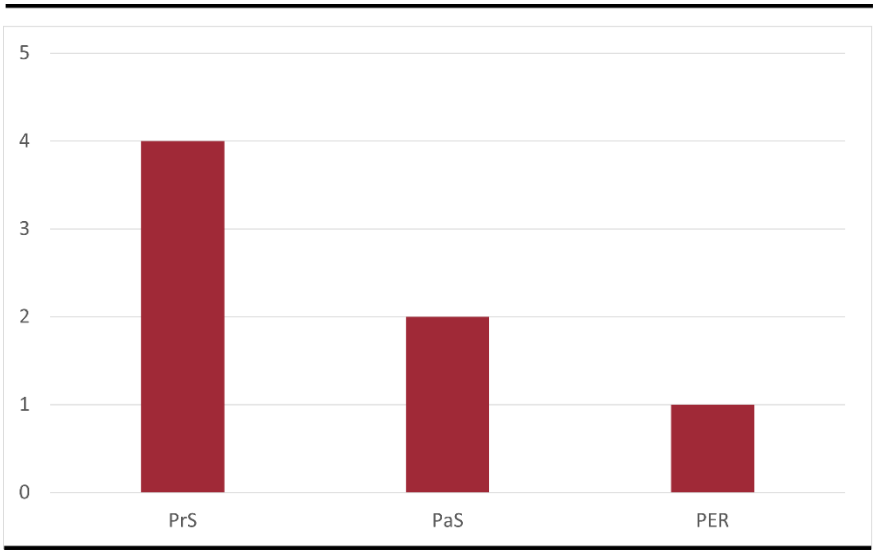

Figure 17. **The distribution of monosynaptically labelled cells in the parahippocampal region.** Four cells were found in the presubiculum (PrS), two cells in the parasubiculum (PaS) and one cell in the perirhinal cortex (PER).

In the PrS, the cells were found in the very dorsal region, and they were situated in the superficial layers. Moreover, the cells were found close together in a cluster, not scattered throughout in the region (Figure 18, F and G). The two cells in the PaS were confined to the deep layers close to the border of the MEC (Figure 18, D, blue square). As shown in figure 18 G, the area surrounding the cells was highly auto-fluorescent. Thus, the cells were hard to discern from their surroundings. In the PER the single identified cell was weakly fluorescent. This cell was found in the deep layers of the PER, close to the white matter (Figure 18, C).

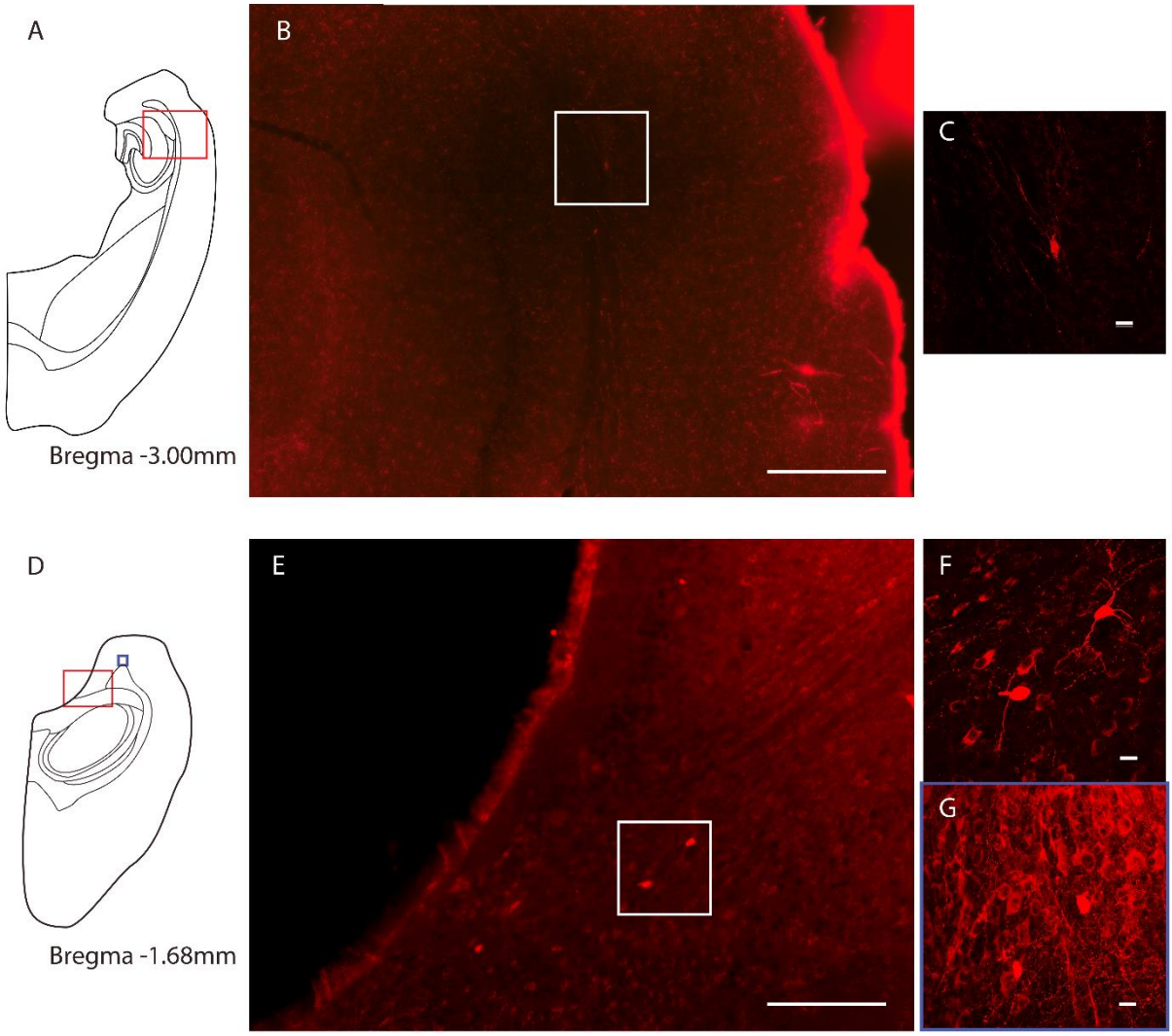

Figure 18. **Representative mCherry labelled cells in the parahippocampal region.** Monosynaptically mCherry labelled cells from rabies tracing in the MEC are displayed in the images. A) A schematic overview of the approximate position of the cell in the PER. The red square represents the image in B. B) An overview of the area in the MEC with the labelled cell in PER (Mirax scan 20x magnification). C) Confocal images (40x) of the PER cell showing soma shape and distribution of dendrites. D) A schematic overview of the approximate position of cells in the PrS and the PaS in the dorsal hemisphere. The red square represents the image in E (Mirax scan 20x magnification), while blue square represents the image in G. F) and G) Confocal (40x) images of cells found in the PrS and the PaS respectively. Scale bars in B and E 200µm; scale bars in C and G-H 20µm.

Monosynaptic inputs from the HF

All of the monosynaptically rabies virus traced cells found in the HF were confined to the very dorsal regions. A total of ten labelled cells were detected across all sections of the HF. Nine of these were confined to the CA1, while one cell was found in the CA2 (Figure 19).

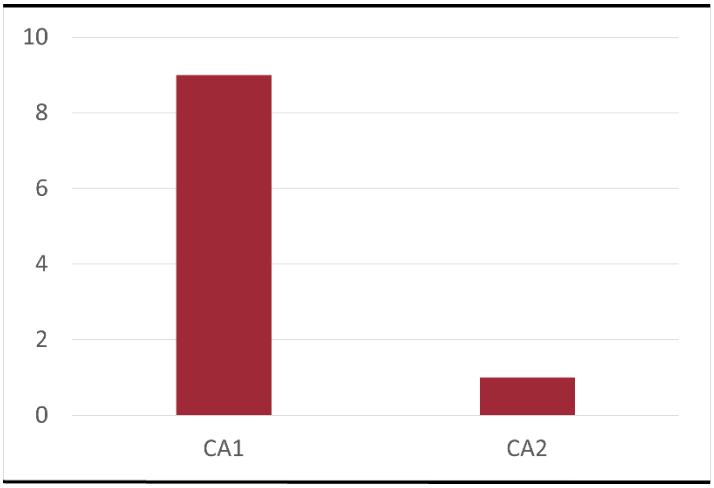

Figure 19. **Distribution of labelled cells across different subregions of the HF.** A total of ten cells were found in the HF, nine cells were located in the CA1 and one cell in the CA2.

Most of the retrogradely labelled cells found in the CA1 were located in the stratum pyramidale, these all had pyramidal soma shapes and dendrites extending into both deeper and more superficial layers (Figure 20, B and D). A few cells were also seen in the stratum radiatum. Cell bodies found in this layer had an ovoid shape, and dendrites extending inside the layer itself. A single cell was seen in the stratum oriens close to the stratum pyramidale. Its cell body was ovoid, and the dendrites seemed to be confined to the same layer as the soma (Figure 20, B).

Only one cell was observed in the CA2 in my experiments. This single cell was located in the stratum oriens, directly superficial to the stratum pyramidale. Its cell body was ovoid, and the dendrites seemed to be confined to the same layer as the soma (Figure 20, B and C). The cell

resembled the stratum oriens cell found in the CA1. Many neurites from somata in adjacent sections could also be observed in the dorsal hippocampus, figure 20 B.

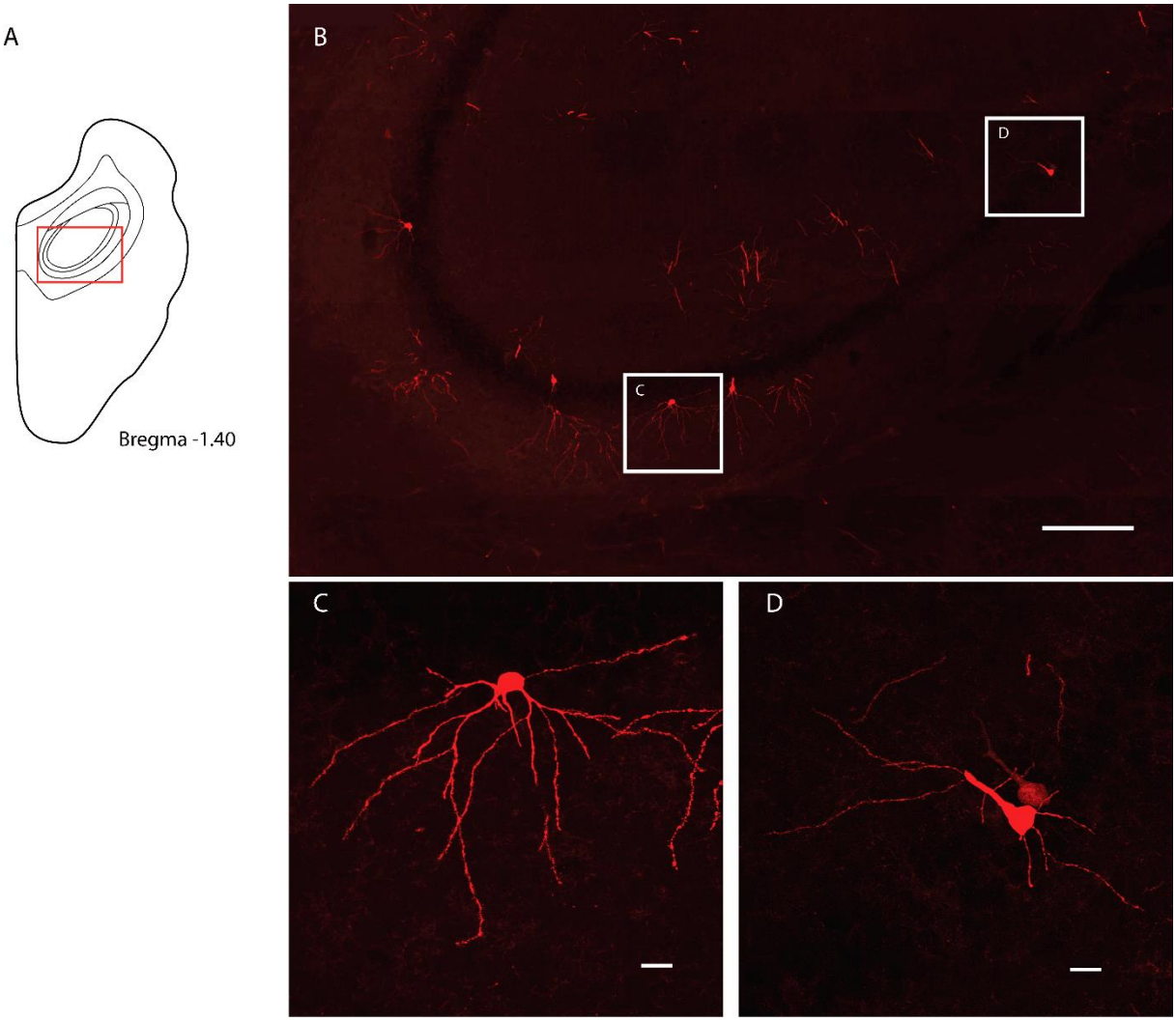

Figure 20. **Representative mCherry labelled cells in the dorsal hippocampus.** Monosynaptically mCherry labelled cells from rabies tracing in the MEC are displayed in the images. A) A schematic overview of the approximate position of cells in the CA regions. The red square represents the image in B. B) An overview of the CA (Mirax scan 20x magnification). C) Confocal image (40x) of a CA2 cell showing the soma shape and distribution of dendrites. D) Confocal image (40x) of a CA1 cell showing the soma shape and distribution of dendrites. Scale bars in B and E 200µm; scale bars in C-D and F 20µm.

Monosynaptic inputs from neocortical and subcortical structures

As the traced input was rather sparse, only a few inputs cells were seen in areas outside the HF and the PHR. A total of five cells were found in neocortical and subcortical areas. Two of these

cells were seen in the ventral RSC. The only subcortical structure represented in the data was the medial septum, where 3 cells were counted (Figure 21).

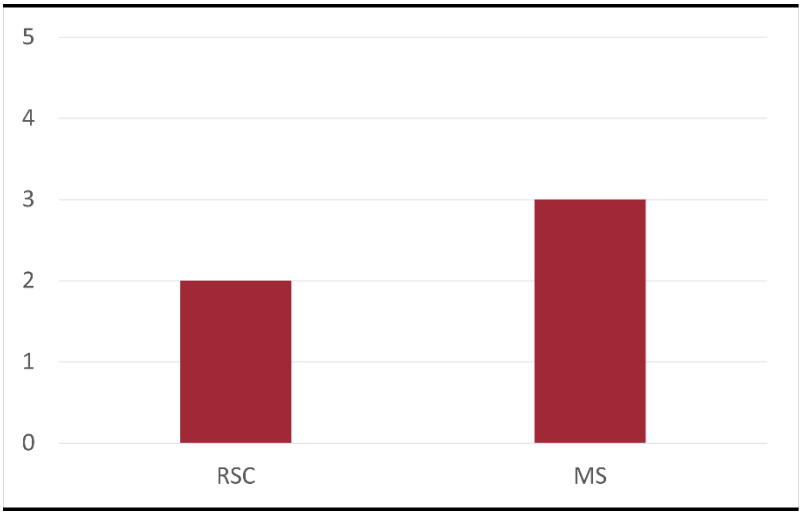

Figure 21. **The distribution of monosynaptically labelled cells in the neocortex and subcortical structures.** Two cells were found in the retrosplenial cortex (RSC) and three in the medial septum (MS).

In the RSC both cells were located ventrally (Area 29a, Figure 22 A-B), in superficial layers. They were strongly fluorescent with easily discernable somata and neurites. Both cells were pyramidal in their shape, with clear thick apical dendrites and several thinner basal dendrites extending from the somata (Figure 22 C). The cells found in the medial septum were located in

intermediate parts of the structure (Figure 22 D), they all had triangular soma shapes with dendrites extending in all directions (Figure 22 E-F).

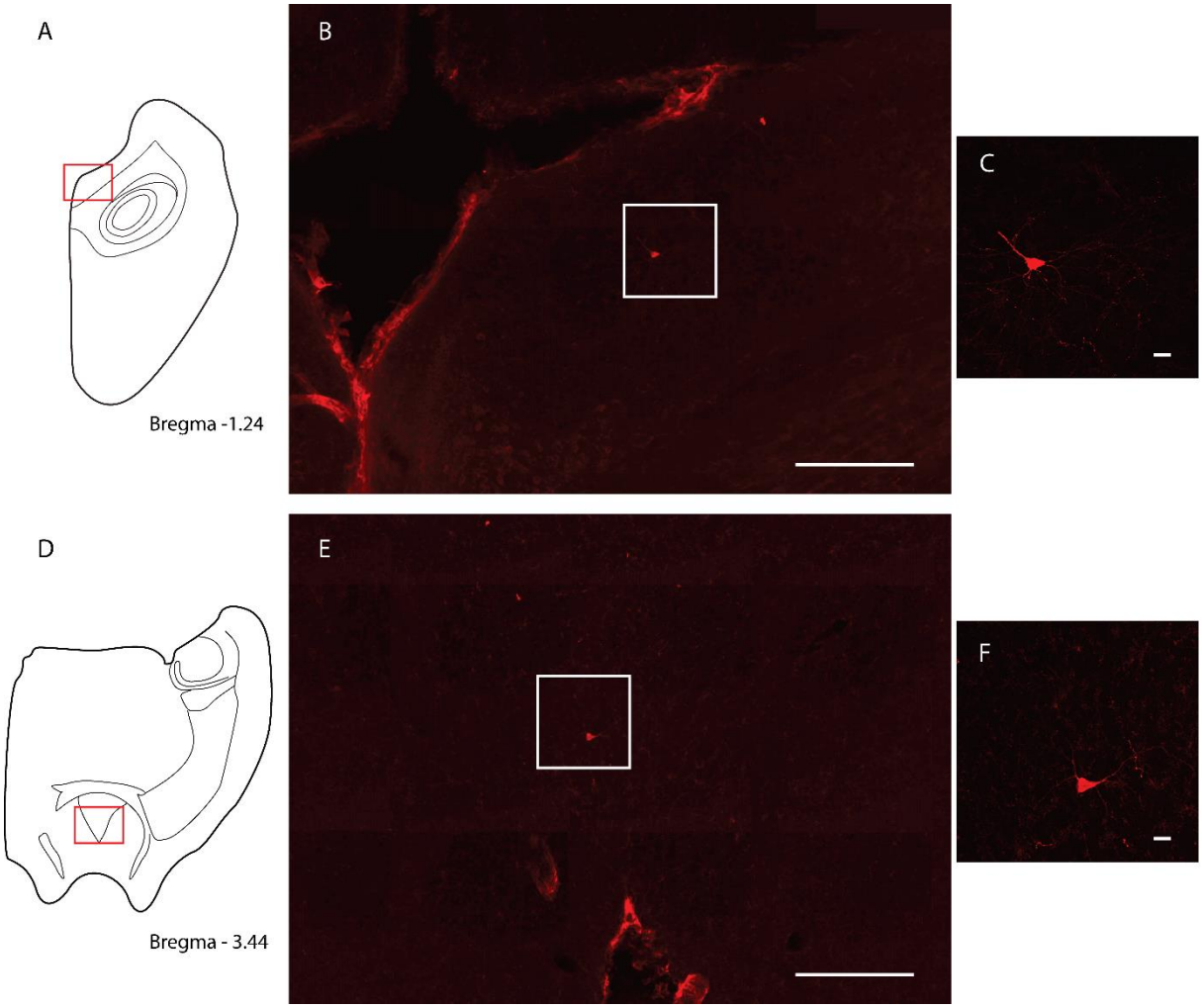

Figure 22. **Representative mCherry labelled cells in the retrosplenial cortex and the medial septum.** Monosynaptically mCherry labelled cells from rabies tracing in the MEC are displayed in the images. A) A schematic overview of the approximate position of cells in the RSC and the dorsoventral level of the section. The red square represents the image in B. B) An overview of the area in the RSC with a labelled cell (Mirax scan 20x magnification). C) Confocal image (40x) of the RSC cell in B showing the soma shape and distribution of dendrites. D) An overview of the ventral section where cells were found in the MS. The red square illustrates the position of a single MS cell shown in E. E) An overview of the area in the MS with a labelled cell (Mirax scan 20x magnification) F) Confocal (40x) image of the cell in E showing cell shape and dendrite distribution. Scale bars in B and E 200µm; scale bars in C and F 20µm.

3.3.2 Intrinsic connectivity of SST cells in the medial entorhinal cortex

A total of four animals had local transport of the rabies virus within the MEC itself. One of the brains could not be quantified due to problems with the IHC against the molecular tag (HA-tag) carried by the helper virus. Hence, it was not possible to separate the starter cell population from the monosynaptically labelled cells, Therefore, only three brains were used to characterize the distribution of monosynaptically labelled cells in the MEC.

Starter cell populations and monosynaptic inputs in the medial entorhinal cortex

All injections were made in the dorsal extreme of the MEC, hence, all starter populations were confined to dorsal regions of the MEC. The starter cells were defined as cells that expressed both the tag from AAV helper virus (either a GFP or HA-tag) and the fluorescent protein from the rabies virus (either GFP or mCherry). In two of the cases a large amount of the starter cells were limited to the superficial layers LII and LIII. In all the cases described, local monosynaptic transport was also largely confined to superficial layers. In figure 23, the different cases with local monosynaptic cells (either GFP or mCherry) are shown. The laminated distribution of starter cells is shown in the right column, while local monosynaptic cells are shown in the left column.

The case shown in figure 23 A and B (no. 52211, red) stood out compared to the other cases. Its starter cells shown in A, were mostly confined to deeper layers, especially LV seemed to be dominant. However, a few starter cells were also found in superficial layers (Figure 23 A). Almost all the monosynaptically labelled cells were identified in LIII, and only a few cells were seen in other layers, figure 23 B. This was the same case that also had long-distance transport) described in section 3.3.1).

Figure 23 C and D shows the distribution of starter cells and monosynaptic cells from the other case (no. 54799, yellow) that only showed sparse intrinsic monosynaptic labelling. The whole starter population was confined to superficial layers (LII and LIII), with LII as the dominant layer (Figure 23 C). Superficial layers were also the dominant with regards to the local monosynaptic input cells, where LIII had the largest count of cells, figure 23 D. Only two monosynaptic cells were found in deeper layers (Figure 23 D).

The third case with monosynaptic intrinsic transport (no. 53586, blue) shown in figure 23 E and F had the largest population of starter cells, but the lowest amount of monosynaptically traced

cells. Essentially all the starter cells were confined to superficial layers. Just like the previous case, most starter cells were found in LII and LIII (Figure 23, E). Only one starter cell could be identified in deeper layers. Monosynaptically labelled cells were found evenly distributed in superficial and deep layers, but very few cells had been traced compared to other cases (Figure 23 F).

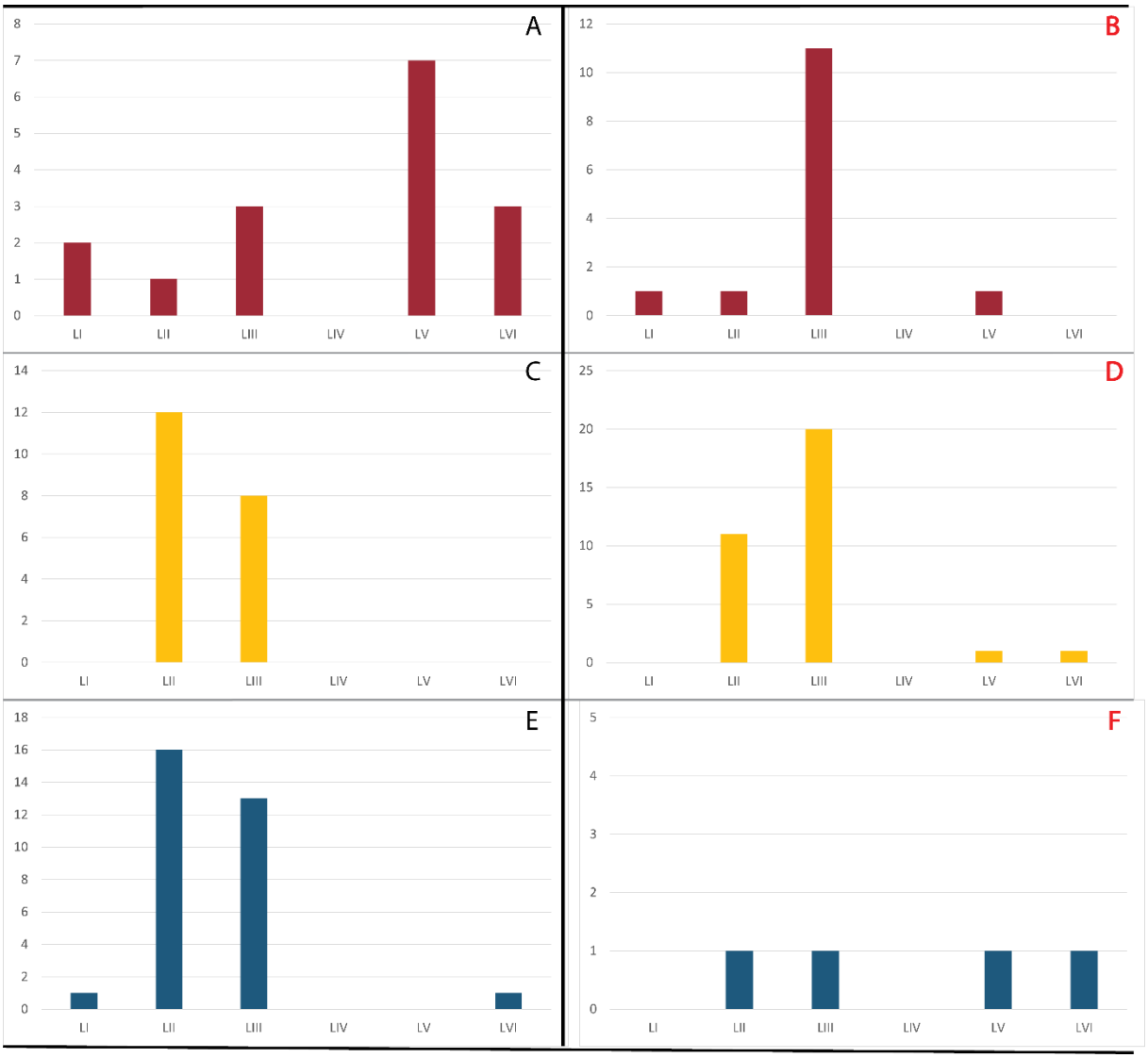

Figure 23. **Histograms with the layered distribution of starter cells and monosynaptic cells.** Cells from three different animals. A), C) and E) with black letters show the layered distribution starter cells within the MEC. B), D) and F) with red letters show the layered distribution of local monosynaptic cells from within the MEC.

Figure 24 shows an example image of MEC cells that have been traced monosynaptically. A dorsal section of the MEC (level shown in fig. 24 A, red square), contains a traced neuron (fig 24 B, white square and fig 25 C magnification). Although this cell was located in deep layers,

most of the cells were actually found in superficial layers. A last note is that labelling of non-neuronal cells was observed in the MEC (Figure 24, blue square). These seemed to reside close to the injection site and were identified as clouds of fluorescence.

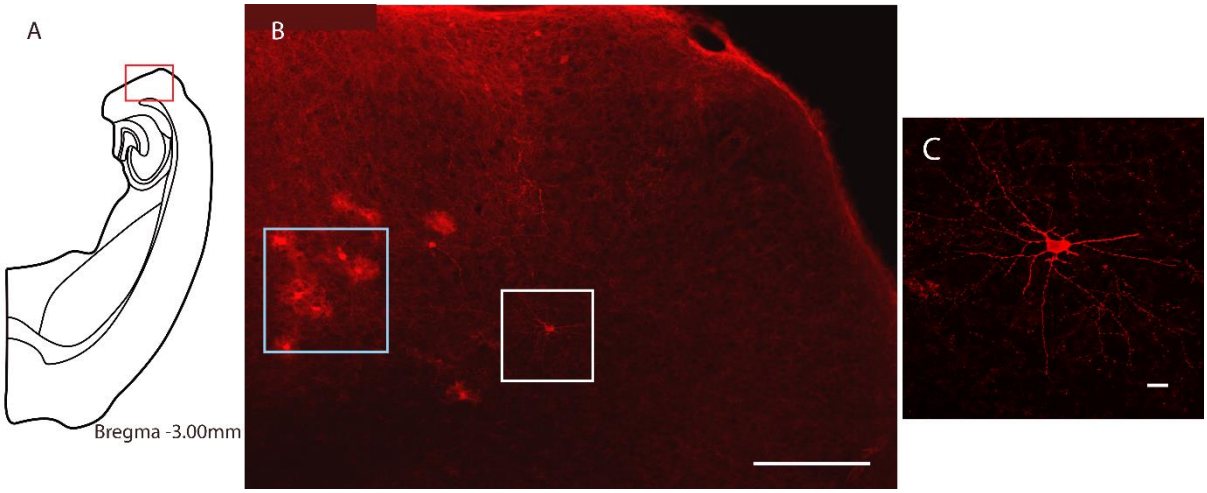

Figure 24. **Representative mCherry labelled cells in the medial entorhinal cortex.** Local monosynaptic labelled mCherry cells in the MEC. A) A schematic overview of the approximate position of a cell in the MEC in an intermediate section. The red square represents the image in B. B) An overview of the area in the MEC with a fluorescent cell in the white square (Mirax scan 20x magnification) as well as a couple of non-neuronal cells in turquoise square C) Confocal image (40x) of the MEC cell shown in B showing soma shape and extension of dendrites. Scale bars in B 200µm; scale bars in C 20µm.

3.4 Anterograde fibers originating in the MEC

One of the monosynaptically traced animals showed unusual anterograde fiber labelling with origins in the MEC. Figure 25 shows strong fiber labelling in several brain areas, including the HF (Figure 25 A), the dorsal perforant path (Figure 25 E). Layer II of the MEC ipsilateral to the injection had strong fiber labelling, but also a few GFP expressing somata in certain regions (Figure 25 C). Fibers were also found in LI and LV of the ipsilateral MEC, but this fiber staining was sparser. Figure 25 B also shows a few fibers in the contralateral MEC. They made a weak plexus in the superficial layers, with a few fibers in the deep layers. The ipsilateral intermediate PaS also had strong fiber labelling, which was mainly confined to the superficial layers (Figure 25, D).

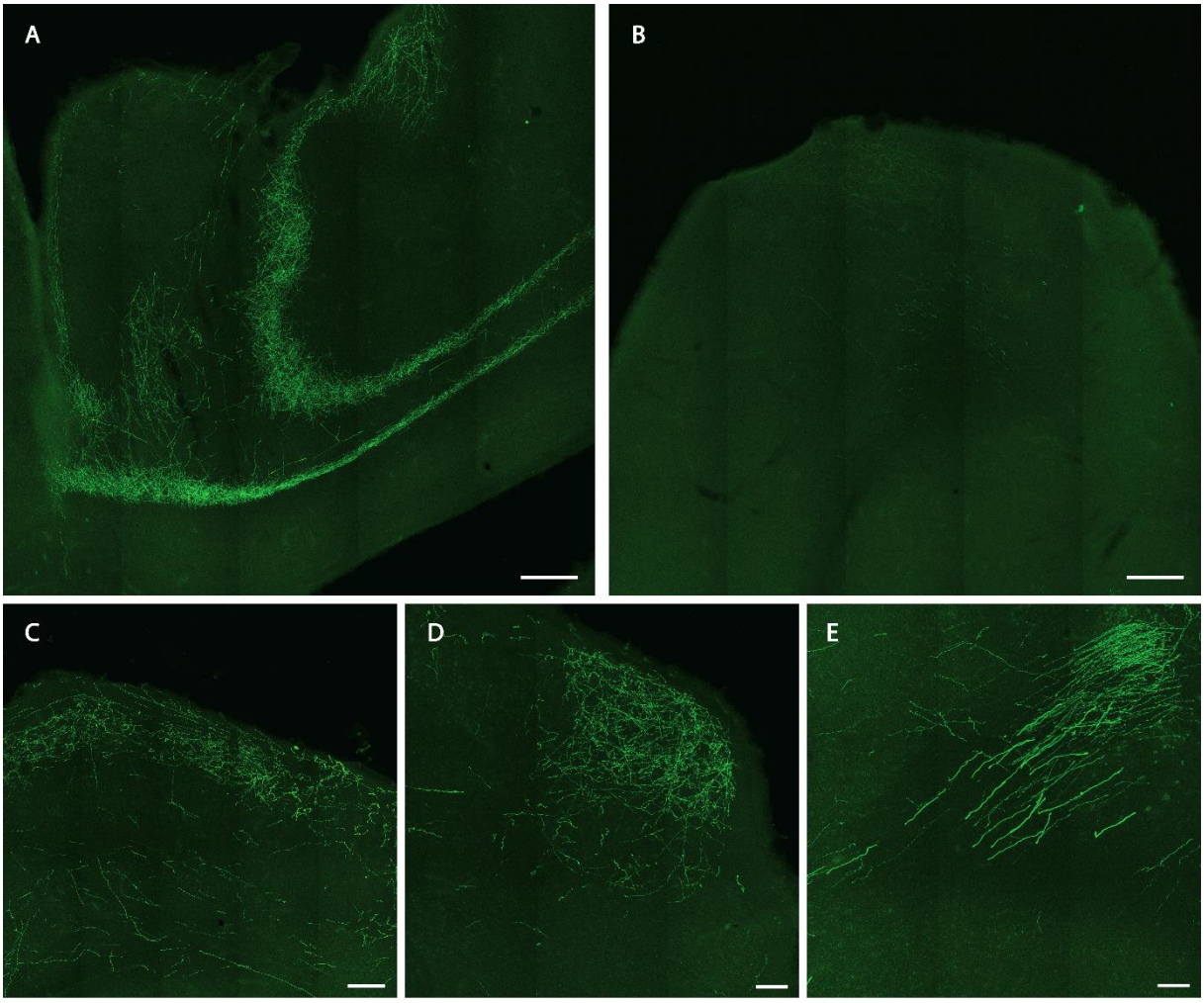

Figure 25. **Anterogradely traced fibers from the MEC.** GFP labelled fibers from a rabies injection in the MEC. A) Overview of the ipsilateral dorsomedial HF with GFP expressing fibers. B) Labelled fibers in the contralateral MEC. C) Fibers in the ipsilateral MEC with a prominent LII plexus. D) Fibers in the parasubiculum. E) Fibers in the CL perforant pathway. Scale bars in A and B 200µm; Scale bars in C 100µm; Scale bars in D and E 50µm.

Chapter 4 Discussion

4.1 Methodological Considerations

4.1.1 SST cells and microscopy

The IHC staining against SST did not stain somata to a high degree. A general feature of neuropeptides is their low concentration in cells, likely because the peptides are synthetized in the cell body but immediately packaged into large dense-core vesicles and transported to the axon terminals (Mains & Eipper 1999). Hence, strong axonal labelling and only weak somatic labelling occurs due to the localization of the neuropeptide. Visualization of SST cell somata with regular fluorescent microscopy was difficult because the excitation and detection filters for the light were fairly broad. With only partially stained somata the IHC was often misconceived as artifacts in the tissue, which lead to an underrepresentation of the number of immune positive somata. To overcome this problem, I changed to confocal microscopy. The confocal microscope had more specific excitation wavelengths and more sensitive detection machinery. Moreover single optical section can be made omitting unspecific signals from planes above and below the plane of focus, making it possible to better discern overlapping somata. However, the downside to using confocal microscopy was that it is very time consuming, hence the counted areas were smaller.

4.1.2 Viral tracing

Because the cell-type specific retrograde monosynaptic tracing system was new in my hands, four different experimental protocols were tested in order to optimize monosynaptic transport. This was done while restricting the injections to my area of interest. Injections with moderate volumes, performed over two separate surgeries with long incubation periods generated the best results.

In the first strategy small volumes of both viruses were injected in two surgeries. Both viruses were of low titer, meaning that the injected volume contained a smaller amount of viral particles. The viruses were given a long time to incubate at the injection sites. As only one of four injected cases provided long-distance transport of the rabies virus, I conclude that the strategy was suboptimal. Most likely this was a complication of small volumes injected and low viral titers. It may also have been caused by the small volumes being injected separately, as it

could have displaced the injections relative to each other. Thus barring the rabies virus from infecting starter cells.

In the second strategy, the AAV vector was changed into a vector containing a different G-protein to the first virus. The new G-protein was thought to improve monosynaptic transfer and was used in the remainder of the experiments (Ghanem & Conzelmann 2016). A mixed strategy with small volumes was chosen in an attempt to make it easier to confine the injection to a restricted region. In order to save time, the viruses were given a short incubation period. However, only one of four infected cases gave us results, indicating that the strategy was less preferable. This was likely a combined effect of the short incubation period and the mixing of the viruses. The short incubation period could result in less AAV expression in the infected cells (Aschauer et al. 2013). Also, due to the high replication rate of G-deleted rabies virus (Morimoto et al. 1998; Ohara et al. 2013), it might prevent the AAV from replicating blocking its expression of vital proteins.

The third set of infections used a similar strategy. Combined with longer incubation period, eight cases were injected with a larger volume of virus. Better viral expression and monosynaptic transport was seen, as four of eight cases gave us viral transport, two of these were found to be long-distance. Nevertheless, two of the cases had misplaced injections, most likely a complication of large volumes of viral tracer making it harder to confine it to a small region. As the rabies virus have been found to kill cells with longer incubation periods (Wickersham et al. 2007), the long incubation period could have killed some of the starter cells, hampering the monosynaptic transport. For unclear reasons, the viral expression seemed to be worse in the MEC.

The fourth strategy turned out to give the best viral expression. Both viruses were injected at separate time periods and the AAV virus was given a longer incubation time. The viruses were injected at moderate volumes, thereby increasing the chance to hit same the spot with both injections. All the analyzed cases gave us good viral expression and transport, indicating an optimal strategy. However, one of the viral injections was misplaced. A small injection placed wrongly might not spill into the area of interest, while a larger injection might. As this injection was of moderate size, the misplaced injection might not have spilled into the area of interest and expression outside the designated area occurred. In the MEC, I observed a strange viral expression, as the rabies virus seemed to have transported anterogradely. This have also been

reported in sensory neurons (Callaway & Luo 2015). Although the explanation for this expression is unclear, this viral strategy seemed to give the best result.

There are several limitations to the use of a monosynaptic viral tracing system for mapping the inputs to particular cell groups in the brain. The number of input cells seen per starter cell in this particular study, and other studies with higher yield, is low. It have been discussed that starter cells most likely only reflect a fraction of the inputs (Wall et al. 2010; Callaway & Luo 2015). This is a probable scenario for us since I observe an approximately 1:1 ratio between starter cells and rabies cells. Hence, the labeled cells will give us an underrepresentation of the actual number of inputs, but also a potential misrepresentation of the areas connected to the cells in my starter population. Moreover, one might expect that the number of inputs per starter cell would go down in case of a larger starter population. If the starter population is very small, like the ones in this thesis, it is possible that the number of viral particles in the infected area is small and this would be a limiting factor to the rabies transport. It is also conceivable that as the starter population grows I will see more input cells that actually project to more than one starter cell. However, since my small starter population might reflect a low amount of viral particles in the region, such divergent input would not be detected in the current system. Although, I do not know the reason why certain inputs are traced and others are left out. In conclusion, the efficacy of the monosynaptic tracing system will be affected by viral titers, viral volumes, incubation times and properties of the viruses that remain unknown.

4.2 Mouse line specificity

The overlap between the transgene expression in the mouse line and the IHC stain against SST was found to be high, approximately 83%. There are a few reasons why the overlap between the transgene marker (GFP) and the IHC for SST was not closer to 100%. First, the IHC staining against SST did not stain somata to a high degree. This may have caused somata of SST positive cells to display only weak or no staining, and SST cells could have been missed in the counts. Second, cre-dependent reporter viruses can potentially express their payload in non-cre cells (Sun et al. 2014). The virus was previously tested for such expression in my lab, and it did not show nonspecific expression (Bente Jacobsen, pers comm). Cre-recombinase may also be expressed in cells that do not express SST due to insertional effects from the generation of the transgenic mouse line, hence a small number of non-SST cells probably express the Cre-recombinase (Hu et al. 2013)

4.3 Distribution of SST cells in the MEC

The SST cells were distributed relatively evenly across the dorso-ventral axis of the MEC, although the dorsal section seemed to have marginally more cells than the two other sections counted. Although the total numbers of SST neurons in the different cell layers apparently did not differ when normalized to surface area, it became clear that the deep layers contain higher numbers of SST neurons than the superficial layers.

There has been a few reports about the distribution of SST interneurons in rats, however there is little literature from mice showing the basic distribution of SST cells in the entorhinal cortex (Köhler & Chan-Palay 1983; Wouterlood & Pothuizen 2000). The studies from rats vary in their observations, Köhler (1983) supports my finding that more SST cells are situated in deeper layers compared to superficial layers. However, Wouterlood (2000) reported the opposite; more SST cells in the superficial layers. Unlike these studies, I normalized to area size. Thus, there might be some discrepancies when I compare our results. If I compare the distribution of SST cells in the MEC with other cortical regions such as the somatosensory cortex (Morrison et al. 1983), the PrS (Nassar et al. 2015) and the lateral entorhinal cortex (Phan 2015; Jordheim 2016), they show similar distributions to the one reported here, having the highest cell counts in deep layers. Thus the laminar distribution of SST cells complements that of PV interneurons, which have been found to be more confined to the superficial layers of the MEC (Wouterlood et al. 1995; Miettinen et al. 1996). Based on these reports, it is reasonable to believe that there is a differential distribution of GABAergic cells in the MEC. Taken together, my findings and previous reports in the literature indicate that the distribution of SST cells is consistent throughout the cortex.

4.4 Monosynaptic inputs to somatostatin interneurons in the MEC

4.4.1 Extrinsic inputs to somatostatin interneurons in the MEC

Monosynaptic inputs to SST cells in the MEC were found to originate in subregions of the HF and the PHR as well as in the RSC and the MS. The local monosynaptic connectivity seemed to be confined to superficial layers of the MEC with few input cells located in the deeper layers. An overview of the monosynaptic inputs is found in figure 26, below.

The monosynaptic inputs from the HF were relatively strong compared to inputs from other regions. Projecting cells were found only in dorsal regions of the HF, a finding that corresponds well with my injection site being located at the dorsal extreme of the MEC (Cenquizca & Swanson 2007). Projections from the CA1 and CA2 target SST cells, but also the general cell population (Cenquizca & Swanson 2007; Rowland et al. 2013). The projection from the CA1 to the MEC is thought to be stronger than the projection from the CA2 (Agster & Burwell 2013), and they seemingly target separate layers. Strikingly, no projections to SST cells were observed from the subiculum, a projection that is known to be of similar strength as the CA1 projection to the MEC, and that terminates with similar topography (Kloosterman et al. 2003). Comparable results were also seen in the LEC in another study in my lab, implicating that there could be a lack of projections from the subiculum to the SST cells in the MEC (Jordheim 2016).

Rabies infected cells were found both in the PrS and the PaS, both are areas known to target several layers of the MEC (Köhler 1985; Caballero-Bleda & Witter 1993; Canto et al. 2012). The PrS proejctions terminate preferentially in LI, III and V (Caballero-Bleda & Witter 1994; van Haeften et al. 1997; Wouterlood et al. 2004), and the projection is known to carry a strong GABAergic component in addition to a glutamatergic one (van Haeften et al. 1997). PV cells have been identified synaptic targets of the GABAergic projection (Wouterlood et al. 1996), however it is conceivable that it also targets other GABAergic populations such as the SST cells. Projections from the PaS to the MEC are known to target LII preferentially, and this could possibly explain the relatively weaker projection from the PaS compared to the PrS based on my starter population being located in LIII and V (Caballero-Bleda &Witter 1994). The projection from the PER to the MEC is relatively weak compared to other projections (Burwell & Amaral 1998b; Agster & Burwell 2013), which is also what I see when looking at the inputs to SST cells. Strikingly, no cells were observed in the POR. This should be expected since the POR have strong input to the dorsocaudal regions of the MEC (Burwell & Amaral 1998a; Burwell & Amaral 1998b). The main input layers of the POR projection is to LI-LIII, which is known to target principal cells in LII of the MEC (Burwell & Amaral 1998b; Koganezawa et al. 2015). Since POR projections terminate strongly in the area of my injection, POR cells either seem not to target SST cells or provide a very weak input to SST cells, not seen in my data.

A few inputs were observed outside of the HF and the PHR in the RSC and the MS. The MS contained a few labelled cells. In the literature, a relatively strong connection from the MS to the MEC has been reported (Alonso et al. 1984; Kondo & Zaborszky 2016). This projection

has been found to contain GABAergic, glutamatergic and cholinergic fibers terminating in all layers of the MEC (Zaborszky et al. 2012; Kondo & Zaborszky 2016). A couple of cells were found in the RSC, an area known to project heavily to the dorsomedial portions of the MEC (Shibata 1994; Jones & Witter 2007; Sugar et al. 2011). The inputs from the RSC targets the deeper layers of the MEC (Jones & Witter 2007), which was the area with the highest number of starter cells in my study.

From the literature, the MEC is known to have inputs from close to all cortical regions, with particularly strong projections from the piriform, temporal and occipital cortices (Burwell & Amaral 1998a; Kerr et al. 2007). Therefore, I should expect to observe cells in these regions, however the cortical inputs to the MEC have a strong topography. Hence, my injection site in the dorsomedial extreme of the MEC may have caused us to see only few of the known connections to the area. Regarding subcortical structures, the amygdala, dorsal thalamus, the claustrum and olfactory nuclei provide strong subcortical inputs to the MEC (Kerr et al. 2007). However, only a weak input from the amygdala is observed in dorsal regions, the same goes for the olfactory nuclei. Although the dorsal midline nuclei and the claustrum have been indicated to provide the dorsal MEC with afferents, no cells were observed in either of the two areas. I still do not know how the rabies virus "selects" presynaptic cells to infect, but the process is limited by the including factors: the levels of G expression in starter cells, numbers of rabies viral particles entering the cells and the incubation time of the virus (Callaway & Luo 2015). Thus, monosynaptic tracing is probably limited to subset of input cells for reasons that are unknown.

Altogether, the monosynaptic inputs to SST cells in the MEC were stronger from the PHR and the HF than from neocortical and subcortical structures. This has also been seen in previous studies of MEC connectivity (Burwell & Amaral 1998a; Burwell 2000; Agster & Burwell 2013).

4.4.2 Intrinsic inputs to somatostatin interneurons in the MEC

When looking at the laminar organization of the starter cells in the MEC, two cases had superficial starter cells and only locally traced cells, and one case had starter cells mainly in deep layers, this case also had traced cells outside the MEC. Regardless of where the starter cells were located, the highest number of local traced cells was seen in the superficial layers, indicating that SST cells are more strongly targeted by inputs from superficial cells, compared

to cells located in deep layers. This was also shown in a recent study of the barrel cortex, suggesting that such preferential input from superficial cortical layers may be a general feature of SST cells (Wall et al. 2016). This is also seen as a general trait for the MEC. Köhler (1986) reported that deep layers project to superficial layers, and that projections originating within superficial layers are confined to superficial layers. Thus, it would seem that SST cells follow the same intrinsic connectivity schema as the general cell population in the MEC. With regards to intrinsic inputs, the SST cells in my study received more projections from cells in superficial layers of the MEC compared to deeper layers, irrespective of the position of the starter cells. Respectively, the SST cells in the MEC seem to have a relatively modest intrinsic input, but the strength of the total extrinsic inputs outweighs the strength of the intrinsic inputs. Although, the SST cells have been reported to receive inputs from about 15% of the principal cells (Jiang, et al. 2015), no reports have directly compared the intrinsic inputs to the extrinsic inputs. Hence, the weak intrinsic inputs reported here, could potentially be unique to the MEC.

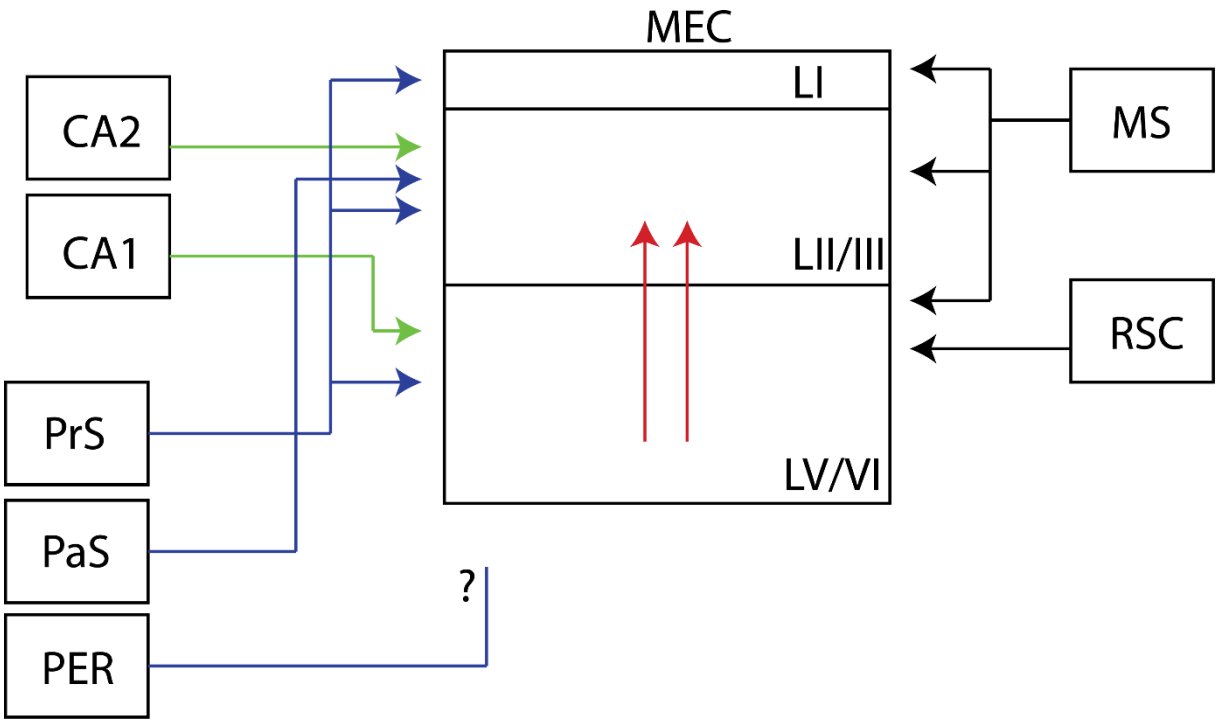

Figure 26. **Overview of the monosynaptic inputs to the SST cells population in the MEC.** Arrows indicate the layers different regions terminate in. Color coding of the arrows indicate input region, black – neocortical and subcortical, blue – the PHR, green – the HF and red – intrinsic projections. For abbreviations, see list of abbreviations.

4.5 Functional implications

The results from the monosynaptic tracing experiments provided us with some interesting insights into the connectivity of SST cells in the MEC. The intrinsic connectivity of the SST cells seems to be weak compared to the extrinsic connections. In fact, less than half of the monosynaptic inputs on to SST cells in the MEC originated from local cells. Interestingly, the the LEC did show a stronger intrinsic input (Jordheim 2016). This suggests that the SST cells in MEC are dominated by inputs arising from extrinsic sources, and that intrinsic inputs play a less significant role in controlling SST cell activity. A study looking at PV cells in the MEC showed similar results (Bente Jacobsen, unpublished data). Although the function of this preferred input connectivity is unknown, it suggests that the information processed in the local circuit of the MEC reflects extrinsic inputs to a great extent. I do not know whether the weak intrinsic input is specific for the SST (and PV) cells or if this is the general organization of the local circuitry in the MEC. However, this might provide the first evidence that the MEC has a connectivity that is extraordinary.

From functional studies, the grid cell have been found to be most numerous in superficial layers of the MEC (Boccara et al. 2010). They are suggested to be an important component in spatial navigation (Fyhn et al. 2004; Hafting et al. 2005). The underlying circuits causing these spatial cell properties have not yet been elucidated. However, it has been suggested that interneurons are important for information processing in these local circuits (Couey et al. 2013). Although the function of the SST cells in this context remains unknown, it has recently been shown that they have preferential connections with LII principal cells in the MEC (Fuchs et al. 2016). Since my local monosynaptic inputs were largely confined to superficial layers, it is conceivable that the SST cells are involved with the spatial processing in these layers.

4.6 Future directions

The results presented in this thesis characterize the SST cells in the MEC by immunohistochemistry and describes their inputs through monosynaptic tracing with rabies virus. I only had one case with long-distance rabies virus transport confined to the dorsomedial MEC with input characteristics that differed compared to the general input to the MEC (no POR, PER inputs and no subiculum). Thus, there would be a need for more viral experiments along the whole extent of the MEC to look for topographical differences, and to completely characterize the monosynaptic inputs to the SST cells.

Although my data suggest that the SST cell population in the MEC is similar to the SST cells in the neocortex, it is not possible to grasp their functional circuit properties in the MEC from this data only. To achieve more understanding about their function role, morphological and electrophysiological analyses could be run to improve the classification of the SST cell. This could better explain their functional properties and possibly give the opportunity to compare them to neocortical SST cells.

Moreover, SST cells are only one of three big interneuronal groups by biochemical classification. To understand the connectivity in the microcircuitry of the MEC there seems to be a need to better understand the individual subgroups. Similar analysis on other cell groups should be run to characterize their intrinsic and extrinsic projections Thus, making it possible to compare between subgroups of cells if they exhibit the same weak intrinsic input in the MEC, as was seen for the SST cells, and if they receive specific projections from extrinsic sources that do not match those of the entire MEC.

Chapter 5 Conclusion

In this thesis I have shown that the SST cells are confined to deeper layers of the MEC when considering the size of the area counted. Long-distance monosynaptic inputs to SST cells were identified from the HF, the PHR, and the MS and the RSC. SST interneurons seemed to receive stronger inputs from the HF and the PHR than from neocortical and subcortical regions. Strikingly, no inputs were seen to originate in the subiculum, implicating that there might be preferential input from the CA1. The SST-Cre mouse line was found to be highly specific for SST cells and the monosynaptic tracing worked best with separate injections of moderate volume and long total incubation time. The SST cells in the MEC were found to receive weak intrinsic input and more extensive extrinsic input, suggesting a unique local input connectivity in the MEC microcircuit.

Bibliography

Agster, K.L. & Burwell, R.D., 2009. Cortical efferents of the perirhinal, postrhinal, and entorhinal cortices of the rat. *Hippocampus*, 19(12), pp.1159–1186.

Agster, K.L. & Burwell, R.D., 2013. Hippocampal and subicular efferents and afferents of the perirhinal, postrhinal, and entorhinal cortices of the rat. *Behav Brain Res*, 254, pp.50–64.

Alonso, A., Köhler, C. & Kohler, C., 1984. A study of the reciprocal connections between the septum and the entorhinal area using anterograde and retrograde axonal transport methods in the rat brain. *J Comp Neurol*, 225(3), pp.327–343.

Amaral, D. & Lavenex, P., 2007. Hippocampal Neuroanatomy. In P. Andersen et al., eds. *The Hippocampus Book*. Oxford: Oxford University Press.

Aschauer, D.F., Kreuz, S. & Rumpel, S., 2013. Analysis of Transduction Efficiency, Tropism and Axonal Transport of AAV Serotypes 1, 2, 5, 6, 8 and 9 in the Mouse Brain J. Qiu, ed. *PLoS ONE*, 8(9), p.e76310.

Ascoli, G.A. et al., 2008. Petilla terminology: nomenclature of features of GABAergic interneurons of the cerebral cortex. *Nat Rev Neurosci*, 9(7), pp.557–568.

Beaulieu, C., 1993. Numerical data on neocortical neurons in adult rat, with special reference to the GABA population. *Brain Research*, 609(1-2), pp.284–292.

Berger, T.K. et al., 2010. Brief bursts self-inhibit and correlate the pyramidal network. *PLoS Biology*, 8(9).

Berger, T.K. et al., 2009. Frequency-dependent disynaptic inhibition in the pyramidal network: a ubiquitous pathway in the developing rat neocortex. *The Journal of physiology*, 587(Pt 22), pp.5411–5425.

Boccara, C.N. et al., 2015. A three-plane architectonic atlas of the rat hippocampal region. *Hippocampus*, 25(7), pp.838–857.

Boccara, C.N. et al., 2010. Grid cells in pre- and parasubiculum. *Nature Neuroscience*, 13(8), pp.987–994.

Burwell, R.D., 2000. The parahippocampal region: corticocortical connectivity. *Ann N Y Acad Sci*, 911, pp.25–42.

Burwell, R.D. & Amaral, D.G., 1998a. Cortical afferents of the perirhinal, postrhinal, and entorhinal cortices of the rat. *J Comp Neurol*, 398(2), pp.179–205.

Burwell, R.D. & Amaral, D.G., 1998b. Perirhinal and postrhinal cortices of the rat: interconnectivity and connections with the entorhinal cortex. *J Comp Neurol*, 391(3), pp.293–321.

Caballero-Bleda, M. & Witter, M.P., 1994. Projections from the presubiculum and the parasubiculum to morphologically characterized entorhinal-hippocampal projection neurons in the rat. *Exp Brain Res*, 101(1), pp.93–108.

Caballero-Bleda, M. & Witter, M.P., 1993. Regional and laminar organization of projections from the presubiculum and parasubiculum to the entorhinal cortex: An anterograde tracing study in the rat. *Journal of Comparative Neurology*, 328(1), pp.115–129.

Callaway, E.M. & Luo, L., 2015. Monosynaptic Circuit Tracing with Glycoprotein-Deleted Rabies Viruses. *J Neurosci*, 35(24), pp.8979–8985.

Canto, C.B. et al., 2012. All layers of medial entorhinal cortex receive presubicular and parasubicular inputs. *J Neurosci*, 32(49), pp.17620–17631.

Canto, C.B., Wouterlood, F.G. & Witter, M.P., 2008. What does the anatomical organization of the entorhinal cortex tell us? *Neural Plasticity*, 2008, p.381243.

Cappaert, N.L.M., Van Strien, N.M. & Witter, M.P., 2015. Chapter 20 - Hippocampal Formation A2 - Paxinos, George. In *The Rat Nervous System (Fourth Edition)*. San Diego: Academic Press, pp. 511–573.

Cenquizca, L.A. & Swanson, L.W., 2007. Spatial organization of direct hippocampal field CA1 axonal projections to the rest of the cerebral cortex. *Brain Research Reviews*, 56(1), pp.1–26.

Couey, J.J. et al., 2013. Recurrent inhibitory circuitry as a mechanism for grid formation. *Nature neuroscience*, 16(3), pp.318–324.

DeFelipe, J. et al., 2013. New insights into the classification and nomenclature of cortical GABAergic interneurons. *Nat Rev Neurosci*, 14(3), pp.202–216.

Doeller, C.F., Barry, C. & Burgess, N., 2010. Evidence for grid cells in a human memory network. *Nature*, 463(7281), pp.657–61.

Dolorfo, C.L. & Amaral, D.G., 1998. Entorhinal cortex of the rat: Organization of intrinsic connections. *Journal of Comparative Neurology*, 398(1), pp.49–82.

Druga, R., 2009. Neocortical inhibitory system. *Folia Biol (Praha)*, 55(6), pp.201–217.

Franklin, K.B.J. & Paxinos, G., 2007. *The Mouse Brain in Stereotaxic Coordinates* 3rd editio., San Diego, USA: Elsevier, Academic Press.

Freund, T.F. & Buzsáki, G., 1996. Interneurons of the hippocampus. *Hippocampus*, 6(4), pp.347–470.

Fuchs, E.C. et al., 2016. Local and Distant Input Controlling Excitation in Layer II of the Medial Entorhinal Cortex. *Neuron*, 89(1), pp.194–208.

Fyhn, M. et al., 2004. Spatial representation in the entorhinal cortex. *Science*, 305(5688), pp.1258–1264.

Ghanem, A. & Conzelmann, K.-K., 2016. G gene-deficient single-round rabies viruses for neuronal circuit analysis. *Virus Research*, 216, pp.41–54.

Grieger, J.C. & Samulski, R.J., 2005. Adeno-associated virus as a gene therapy vector: Vector development, production and clinical applications. *Advances in Biochemical Engineering/Biotechnology*, 99, pp.119–145.

van Haeften, T. et al., 1997. GABAergic presubicular projections to the medial entorhinal

cortex of the rat. *The Journal of neuroscience : the official journal of the Society for Neuroscience*, 17(2), pp.862–874.

van Haeften, T. et al., 2003. Morphological and numerical analysis of synaptic interactions between neurons in deep and superficial layers of the entorhinal cortex of the rat. *Hippocampus*, 13(8), pp.943–952.

Hafting, T. et al., 2005. Microstructure of a spatial map in the entorhinal cortex. *Nature*, 436(7052), pp.801–806.

Harris, K.D. & Mrsic-Flogel, T.D., 2013. Cortical connectivity and sensory coding. *Nature*, 503(7474), pp.51–8.

Hu, H., Cavendish, J.Z. & Agmon, A., 2013. Not all that glitters is gold: off-target recombination in the somatostatin–IRES-Cre mouse line labels a subset of fast-spiking interneurons. *Frontiers in Neural Circuits*, 7(December), pp.1–4.

Insausti, R., Herrero, M.T. & Witter, M.P., 1997. Entorhinal cortex of the rat: cytoarchitectonic subdivisions and the origin and distribution of cortical efferents. *Hippocampus*, 7(2), pp.146–183.

Jiang, X. et al., 2015. Principles of connectivity among morphologically defined cell types in adult neocortex. *Science*, 350(6264), p.aac9462.

Jones, B.F. & Witter, M.P., 2007. Cingulate cortex projections to the parahippocampal region and hippocampal formation in the rat. *Hippocampus*, 17(10), pp.957–976.

Jordheim, G.K., 2016. *A characterization of the somatostatin cell population in the lateral entorhinal cortex of the mouse*. Master's Thesis, Norwegian University of Science and Technology.

Kapfer, C. et al., 2007. Supralinear increase of recurrent inhibition during sparse activity in the somatosensory cortex. *Nature neuroscience*, 10(6), pp.743–53.

Kerr, K.M. et al., 2007. Functional neuroanatomy of the parahippocampal region: the lateral and medial entorhinal areas. *Hippocampus*, 17(9), pp.697–708.

Killian, N.J., Jutras, M.J. & Buffalo, E.A., 2012. A map of visual space in the primate entorhinal cortex. *Nature*, 491(7426), pp.761–764.

Kleinknecht, A., 2003. 1. *International Journal of Innovation Management*, 7(3), pp.1–30.

Klink, R. & Alonso, A., 1997. Morphological characteristics of layer II projection neurons in the rat medial entorhinal cortex. *Hippocampus*, 7(5), pp.571–583.

Kloosterman, F., Witter, M.P. & Van Haeften, T., 2003. Topographical and laminar organization of subicular projections to the parahippocampal region of the rat. *Journal of Comparative Neurology*, 455(2), pp.156–171.

Koganezawa, N. et al., 2015. Excitatory Postrhinal Projections to Principal Cells in the Medial Entorhinal Cortex. *J Neurosci*, 35(48), pp.15860–15874.

Kondo, H. & Zaborszky, L., 2016. Topographic organization of the basal forebrain projections to the perirhinal, postrhinal, and entorhinal cortex in rats. *J Comp Neurol*.

Kos, C.H., 2004. Cre/loxP system for generating tissue-specific knockout mouse models. *Nutrition reviews*, 62(6 Pt 1), pp.243–246.

Köhler, C., 1986. Intrinsic connections of the retrohippocampal region in the rat brain. II. The medial entorhinal area. *The Journal of comparative neurology*, 246(2), pp.149–169.

Köhler, C., 1985. Intrinsic projections of the retrohippocampal region in the rat brain. I. The subicular complex. *The Journal of comparative neurology*, 236(4), pp.504–22.

Köhler, C. & Chan-Palay, V., 1983. Somatostatin and vasoactive intestinal polypeptide-like immunoreactive cells and terminals in the retrohippocampal region of the rat brain. *Anatomy and embryology*, 167, pp.151–172.

Lee, S. et al., 2010. The largest group of superficial neocortical GABAergic interneurons expresses ionotropic serotonin receptors. *J Neurosci*, 30(50), pp.16796–16808.

Mains, R.E. & Eipper, B.A., 1999. The Neuropeptides.

Markram, H. et al., 2004. Interneurons of the neocortical inhibitory system. *Nature reviews. Neuroscience*, 5(10), pp.793–807.

Miettinen, M. et al., 1996. Coexistence of parvalbumin and GABA in nonpyramidal neurons of the rat entorhinal cortex. *Brain Research*, 706(1), pp.113–122.

Morales, M. & Bloom, F.E., 1997. The 5-HT3 receptor is present in different subpopulations of GABAergic neurons in the rat telencephalon. *J Neurosci*, 17(9), pp.3157–3167.

Morimoto, K. et al., 1998. Rabies virus quasispecies: implications for pathogenesis. *Proceedings of the National Academy of Sciences of the United States of America*, 95(6), pp.3152–3156.

Morrison, J.H. et al., 1983. Immunohistochemical distribution of pro-somatostatin-related peptides in cerebral cortex. *Brain Research*, 262(2), pp.344–351.

Nagy, A., 2000. Cre recombinase: The universal reagent for genome tailoring. *Genesis*, 26(2), pp.99–109.

Nassar, M. et al., 2015. Diversity and overlap of parvalbumin and somatostatin expressing interneurons in mouse presubiculum. *Frontiers in neural circuits*, 9(May), p.20.

O'Keefe, J., 1976. Place units in the hippocampus of the freely moving rat. *Experimental Neurology*, 51(1), pp.78–109.

O'Keefe, J. & Dostrovsky, J., 1971. The hippocampus as a spatial map. Preliminary evidence from unit activity in the freely-moving rat. *Brain research*, 34(1), pp.171–175.

Ohara, S. et al., 2013. Rabies virus vector transgene expression level and cytotoxicity improvement induced by deletion of glycoprotein gene M. J. Schnell, ed. *PLoS ONE*, 8(11), p.e80245.

Phan, A., 2015. *Immunohistochemical and Morphological Characterization of GABAergic Cells in the Lateral Entorhinal Cortex*. Master's Thesis, Norwegian University of Science and Technology.

Ren, J.Q. et al., 1992. Quantitative analysis of neurons and glial cells in the rat

somatosensory cortex, with special reference to GABAergic neurons and parvalbumin-containing neurons. *Experimental Brain Research*, 92(1), pp.1–14.

Rowland, D.C. et al., 2013. Transgenically targeted rabies virus demonstrates a major monosynaptic projection from hippocampal area CA2 to medial entorhinal layer II neurons. *J Neurosci*, 33(37), pp.14889–14898.

Rudy, B. et al., 2011. Three groups of interneurons account for nearly 100% of neocortical GABAergic neurons. *Dev Neurobiol*, 71(1), pp.45–61.

Sargolini, F. et al., 2006. Conjunctive representation of position, direction, and velocity in entorhinal cortex. *Science*, 312(5774), pp.758–762.

Schnell, M.J. et al., 2009. The cell biology of rabies virus: using stealth to reach the brain. *Nature Reviews Microbiology*, 8(1), pp.51–61.

Scoville, W.B. & Milner, B., 1957. Loss of recent memory after bilateral hippocampal lesions. *The Journal of neuropsychiatry and clinical neurosciences*, 12(1), pp.103–113.

Shibata, H., 1994. Terminal distribution of projections from the retrosplenial area to the retrohippocampal region in the rat, as studied by anterograde transport of biotinylated dextran amine. *Neuroscience Research*, 20(4), pp.331–336.

Silberberg, G. & Markram, H., 2007. Disynaptic Inhibition between Neocortical Pyramidal Cells Mediated by Martinotti Cells. *Neuron*, 53(5), pp.735–746.

Skubis-Zegadło, J., Stachurska, A. & Małecki, M., 2013. Vectrology of adeno-associated viruses (AAV). *Medycyna wieku rozwojowego*, 17(3), pp.202–6.

Solstad, T. et al., 2008. Representation of geometric borders in the entorhinal cortex. *Science*, 322(December), pp.1865–1868.

van Strien, N.M., Cappaert, N.L. & Witter, M.P., 2009. The anatomy of memory: an interactive overview of the parahippocampal-hippocampal network. *Nat Rev Neurosci*, 10(4), pp.272–282.

Sugar, J. et al., 2011. The retrosplenial cortex: intrinsic connectivity and connections with the (para)hippocampal region in the rat. An interactive connectome. *Front Neuroinform*, 5, p.7.

Sun, Y. et al., 2014. Cell-type-specific circuit connectivity of hippocampal CA1 revealed through cre-dependent rabies tracing. *Cell Reports*, 7(1), pp.269–280.

Taniguchi, H. et al., 2011. A resource of Cre driver lines for genetic targeting of GABAergic neurons in cerebral cortex. *Neuron*, 71(6), pp.995–1013.

Taube, J.S., 1998. Head direction cells and the neurophysiological basis for a sense of direction. *Progress in Neurobiology*, 55(3), pp.225–256.

Vogt, B. a. & Vogt, L., 2004. Cingulate Cortex and Disease Models.Pdf. *The rat nervous system (3ed)*, pp.705–727.

Vogt, B.A. & Paxinos, G., 2014. Cytoarchitecture of mouse and rat cingulate cortex with human homologies. *Brain Structure and Function*, 219(1), pp.185–192.

Wall, N.R. et al., 2016. Brain-Wide Maps of Synaptic Input to Cortical Interneurons. *The Journal of Neuroscience*, 36(14), pp.4000–4009.

Wall, N.R. et al., 2010. Monosynaptic circuit tracing in vivo through Cre-dependent targeting and complementation of modified rabies virus. *Proceedings of the National Academy of Sciences of the United States of America*, 107(50), pp.21848–53.

Wang, Y. et al., 2004. Anatomical, physiological and molecular properties of Martinotti cells in the somatosensory cortex of the juvenile rat. *The Journal of physiology*, 561(Pt 1), pp.65–90.

Wang, Y. et al., 2002. Anatomical, physiological, molecular and circuit properties of nest basket cells in the developing somatosensory cortex. *Cerebral cortex (New York, N.Y. : 1991)*, 12(4), pp.395–410.

Wickersham, I.R. et al., 2007. Retrograde neuronal tracing with a deletion-mutant rabies virus. *Nature methods*, 4(1), pp.47–9.

Wouterlood, F.G. et al., 2004. Input from the presubiculum to dendrites of layer-V neurons of the medial entorhinal cortex of the rat. *Brain Res*, 1013(1), pp.1–12.

Wouterlood, F.G. et al., 1995. Parvalbumin-immunoreactive neurons in the entorhinal cortex of the rat: localization, morphology, connectivity and ultrastructure. *Journal of Neurocytology*, 24(2), pp.135–153.

Wouterlood, F.G., Martin-Clemente, B. & Van Haeften, T., 1996. Presubicular axon terminals synapse with parvalbumin-immunoreactive interneurons in the medial entorhinal cortex of the rat. *Soc Neurosci Abstr.*, Vol. 22, p.903.

Wouterlood, F.G. & Pothuizen, H., 2000. Sparse colocalization of somatostatin- and GABA-immunoreactivity in the entorhinal cortex of the rat. *Hippocampus*, 10(1), pp.77–86.

Yartsev, M.M., Witter, M.P. & Ulanovsky, N., 2011. Grid cells without theta oscillations in the entorhinal cortex of bats. *Nature*, 479(7371), pp.103–107.

Yuste, R., 2005. Origin and classification of neocortical interneurons. *Neuron*, 48(4), pp.524–527.

Zaborszky, L., van den Pol, A.N. & Gyengesi, E., 2012. The Basal Forebrain Cholinergic Projection System in Mice. In *The Mouse Nervous System*. pp. 684–718.

Appendix I: List of animals used in experiments

Table 2. **Overview of animals, experiments and outcome of animals with injection in the MEC.** No viral transport means no rabies virus transport. Poor viral transport means local rabies virus transport close to the injection site. Good viral transport means long distance rabies virus transport. See Appendix II for an overview over the strategies

Animal Number	*Experiment*	*Viral labelling*	*Starter cells*	*Viral strategy*
8177	Mouse line specificity and distribution	Good viral expression	Not relevant	Not relevant
52941	Monosynaptic tracing	No viral transport	No	1
52211	Monosynaptic tracing	Good viral transport	Yes	1
52823	Monosynaptic tracing	Poor viral transport	Yes	2
52605	Monosynaptic tracing	No viral transport	No	2
53586	Monosynaptic tracing	Poor viral transport	Yes	3
53047	Monosynaptic tracing	No viral transport	No	3
53588	Monosynaptic tracing	No viral transport	No	3
54799	Monosynaptic tracing	Unusual expression	Yes	4

Appendix II: Viral tracers and viral protocols

Table 3. **Overview of viral tracers, viral protocols and their variables.**

Variables	***Strategy 1***	***Strategy 2***	***Strategy 3***	***Strategy 4***
AAV	AAV5-synP-FLEX-splitTVA-GFP-B19G	AAV2/1-synP-FLEX-splitTVA-2HA-Gcvs	AAV2/1-synP-FLEX-splitTVA-2HA-Gcvs	AAV2/1-synP-FLEX-splitTVA-2HA-Gcvs
Rabies virus	EnvA-pseudotyped, G-deleted rabies mCherry (SADΔG-mCherry)	EnvA-pseudotyped, G-deleted rabies GFP (SADΔG-GFP)	EnvA-pseudotyped, G-deleted rabies mCherry (SADΔG-mCherry)	EnvA-pseudotyped, G-deleted rabies GFP (SADΔG-GFP)
Mix/ratio	-	AAV 2:5, Rabies virus 3:5	AAV:Rabies virus 1:1	-
Amount of AAV	250-300 nL	240 nL	500 nL	400 nL
Amount of Rabies virus	500 nL	360 nL	500 nL	500 nL
Total amount of virus	650-700 nL	600 nL	1 µL	900 nL
Incubation time: AAV	3 weeks	-	-	2 weeks
Incubation time: Rabies virus	1 week	-	-	1 weeks
Incubation time: total	4 weeks	8 days	2 weeks	3 weeks

Appendix III: Surgical procedure and equipment

Surgical Procedure

Surgical Equipment

- Surgery table
- Stereotaxic frame with tower
- Induction chamber
- Heating pad
- Vaporizer unit for isoflurane
- Mask for isoflurane
- Electric razor
- Tweezers
- Two ear bars
- Small surgery scissor
- Clamper
- Stereomicroscope
- Tubes connecting the induction chamber of the mask with the vaporizer unit

  Drill (0.9mm, Foredom Micro Motor FM3545 control and MH-145 Micro Motor Hand piece.

Disposables

- Scalpel (blade 6)
- Isoflurane
- Sterile saline
- Q-tips cotton swabs
- Suture kit
- Syringes
- 27 and 25 gauge needles
- Sugi absorbent swabs (Kettenbach GmbH & Co)
- Ethanol
- Iodine
- Marcain
- Temgesic
- Rimadyl
- Eye oinment

Detailed surgical procedure

Preparation

1. Desinfect the surgery table, microscope and stereotaxic tower with ethanol (70%)
2. Fill up a container with ethanol (70%) and place all the equipment for disinfection
3. Place a sterile piece of paper on the table
4. Find and put the Q-tips cotton swabs, sugi absorbent swabs and the rest of the equipment on the sheet ready for use
5. Prepare small containers with saline and sterile water
6. Prepare syringes with 25 gauge needles for Marcain (Bupivacaine, 1mg/kg, AstraZeneca, UK), Rimadyl and Temgesic (Buprenorphine, 0.05-0.1mg/kg, RB Pharmaceuticals Ltd, USA).
7. Turn on the heating pad and tape a piece of paper on it
8. Fill the vaporizer with isoflurane and make sure all the tubes are placed correctly (turned against the chamber when filling up).

Surgery

1. Clean all surfaces with 70% ethanol
2. Find and prepare necessary surgical equipment
3. Collect the animals from the animal room and weight them before their individual surgery
4. Turn the oxygen flow (1L/min) and isoflurane (5%) and wait for the chamber to be filled (approx. 5 min.)
5. Place the animal in the induction chamber and wait the breathing is slow and deep.
6. Shave the head of the animal
7. Place the animal in the stereotaxic frame; administer isoflurane via the stereotaxic anaesthesia mask
8. Adjust the isoflurane flow to 3%
9. Check for toe-pinch reflexes to be sure that the animal is in deep anaesthesia
10. Subcutaneous injection of Rimadyl and Temgesic, as well as Marcain on the head

11. Apply eye ointment, Simplex (Tubilux Pharma S.p.A., Italy), to prevent the eyes from drying out
12. Fixate the head and make sure that bregma and lambda are in same height and alignment
13. Clean the head with sterile saline, ethanol (70%) and iodine.
14. Check for remaining reflexes
15. Reduce the isoflurane level gradually during the surgery to approx. 1.5%, depending on the animal's breathing rate
16. Carefully look for any abnormalities in breathing pattern throughout the surgery (irregular or slow breathing)
17. Use a scalpel to make an incision along the midline and proceed to remove the periosteum on each side of the skull
18. Use bent needles and tape to keep the skin away from the skull
19. Measure the height level of bregma and lambda with the drill
20. Adjust the skull such that bregma and lambda align in the horizontal plane
21. Use the drill to thin the bone along the midline to reveal the sagittal sinus
22. Carefully drill a small hole to reveal the transverse sinus
23. Use bent needles to remove dura away from the drilling site
24. These reference points together with lambda and bregma served as reference points to calculate injection coordinates
25. Drill a hole in the skull at the injection coordinates
26. Fill the Hamilton syringe with viral tracer (Type of tracer depend on injection protocol. See Appendix XX for more information)
27. Secure the Hamilton syringe in the stereotaxic tower
28. Adjust the needle to the stereotaxic coordinates
29. Lower the Hamilton needle down to the surface of the brain and measure the height
30. Recheck injection coordinates
31. Lower the needle down to the injection site and wait for 2 minutes
32. Inject the virus over a period of 10-15 minutes, depending on the size of injection (See Appendix XX for more information about injection strategies)
33. After injection, keep the needle in place for 10 minutes before slowly raising the needle from the brain tissue
34. Clean the skull with sterile saline after the needle is pulled out

35. Suture the wound and make sure there is no way for the animal to open the stiches by scratching
36. Rinse the suture with sterile saline and dab iodine on the wound to avoid infection
37. Remove the ear bars, turn of the isoflurane and remove the anaesthesia mask.

Post-surgery

1. Wait for the animal to recover from anaesthesia by moving it to a heating-chamber
2. Make baby porridge and place the bowl in the cage
3. Move the animal to its cage
4. Monitor the animal and make sure it can move around and eat
5. Return the cage to the animal room and check the animal an hour after
6. One day post-surgery, a subcutaneous injection of Rimadyl is given to relieve post-surgical pain.

Appendix IV: Immunohistochemistry and Histology

The tissue is washed and incubated at room temperature unless otherwise is specified.

IHC protocol for GFP and mCherry

1. Wash sections in phosphate buffer solution (0.125M) 4x15 minutes
2. Incubate with primary antibody 1:500 in an incubation solution made from: 1% Trx, 0.5% DMSO, 1% NGS in PB 0.125M; 48hrs at 4°C on stirrer.
3. Wash sections in phosphate buffer solution (0.125M) 6x15 minutes
4. Incubate with secondary antibody 1:500 in an incubation solution made from: 1% Trx, 0.5% DMSO, 1% NGS in PB 0.125M; 24hrs at 4°C on stirrer.
5. Wash sections in phosphate buffer solution (0.125M) 5x15 minutes
6. Wash sections in Tris-HCl (pH 7.6) 1x15 minutes
7. Mount and coverslip sections.

IHC protocol for Somatostatin

1. Wash sections in phosphate buffer solution (0.125M) 3 x 15 minutes
2. Antigen retrieval step where the tissue was heated for 2hrs at 60°C in phosphate buffer solution (0.125M)
3. Wash sections in phosphate buffer solution (0.125M) with 1% Triton X-100 (PBT) 2 x 10 minutes for enhanced permeabilization
4. Pre-incubate sections in a blocking solution of PBT with 10% natural donkey serum for 3hrs.
5. Incubate with primary antibody 1:500 in an incubation solution made from: PBT and 10% natural donkey serum; 48hrs at 4°C on stirrer.
6. Wash sections in phosphate buffer solution (0.125M) 4 x 15 minutes
7. Incubate with secondary antibody 1:400 in an incubation solution made from: PBT; 24hrs at 4°C on stirrer.
8. Wash sections in phosphate buffer solution (0.125M) 3 x 15 minutes
9. Wash sections in Tris-HCl (pH 7.6) 1 x 15 minutes
10. Mount and coverslip sections

ICH protocol for HA-tag

1. Wash sections in phosphate buffer solution (0.125M) with 1% Triton x-100 for 4 x 15 minutes
2. Wash sections in Tris (pH 8.0) for 3 x 10 minutes.
3. Wash sections in Tris + 0.5% Triton x-100 to enhance permeabilization.
4. Incubate with primary antibody 1:100 in an incubation solution made from: Tris with 0.5 % Triton x-100 for 4 days at 4°C on stirrer.
5. Wash sections in Tris-HCl (pH 8.0) for 4 x 15 minutes
6. Incubate with secondary antibody 1:400 in an incubation solution made from: Tris with 0.5 % Triton x-100 for 24hrs at 4°C on stirrer.
7. Wash sections in Tris-HCl (pH 7.6) 4 x 15 minutes
8. Mount and coverslip sections

Cresyl Violet

1. Dehydrate sections – 10 dips in each: 50-, 70-, 80-, 90-, 100-, 100-, and 100% ethanol
2. Let sections sit 2 minutes in Xylene for clearing
3. Rehydrate sections – 10 dips in each: 100-, 100-, 100-, 90-, 80-, 70-, and 50% ethanol
4. Quick wash under running water
5. Let sections sit in Cresyl Violet on shaker in dark (time depends on the age of the solution)
6. Let sections sit in running water until all excess color is washed away.
7. Move sections into the Ethanol+Acetic Acid solution for a few seconds, while you gently shake the section holder
8. Move sections quickly to a bath of cold water and let sections sit until all excess color is washed away
9. Repeat point 7) and 8) until the sections are sufficiently light, while the contrast is still good.
10. Dehydrate sections – 10 dips in each: 50-, 70-, 80-, 90-, 100-, 100-, and 100% ethanol
11. Move sections to Xylene baths for clearing. The first bath should be 2 minutes, the second should be at least 5 minutes (up to an hour).
12. Coverslip the sections with entellan in xylene.

Appendix V: Solutions

Ringer

0.85% NaCl	(4.25 g/500 mL H_2O)
0.025% KCl	(0.125 g/500 mL H_2O)
0.02% $NaHCO_3$	(0.1 g/500 mL H_2O)

Place the container with water and a magnet on a stirrer. Add the salts to the water and stir the solution until it is dissolved. Filtrate and heat to 40°C before use. Use O_2 to set the pH to 6.9 and use immediately. Fresh ringer is made before each perfusion.

Phosphate buffer (PB) 0.4M pH 7.4

A: $NaH_2PO_4H_2O$	27.6 g/500 mL H_2O
B: $Na_2HPO_4H_2O$	35.6 g/500 mL H_2O

Make solutions A and B. Add solution A to solution B until the pH is 7.4 (=0.4M). Store in a dark place at room temperature for up to a month.

Note: This is usually made by the lab technicians.

Phosphate buffer (PB) 0.125M pH 7.4

100 mL: 31.25 mL 0.4M PB + 68.75 mL H_2O
500 mL: 156 mL 0.4M PB + 344 mL H_2O

The solution can be stored in refrigerator for up to one week.

10% paraformaldehyde (PFA)

200 mL H_2O
20 g PFA

Microwave the water to 60°C and add the measured PFA to the water. Mix the solution on a hot stirrer with a magnet and add drops of NaOH until the solution is clear. Procedure is carried out in a ventilated hood.

Fixative 4% paraformaldehyde (PFA) 500 mL

200 mL 10% PFA (see above)
156 mL 0.4M PB
144 mL H_2O

Add mixed water and PB to the 10% PFA solution. Adjust the pH to 7.4 by using HCl and filtrate. Procedure is carried out in a ventilated hood. The fixative is one time use and made new for every perfusion.

Dimethyl Sulfoxide solution (DMSO)

31.25 mL 0.4M PB
46.75 mL H_2O
20 mL glycerine
2 mL dimethyl sulfoxide (DMSO)

The solution is mixed under a ventilated hood.

Tris-HCl pH 7.6 500 mL

Tris 3.03g/500mL H_2O

Measure the water and add Tris. Adjust the pH to 7.6 with HCl.
The solution can be stored in refrigerator for up to one week.

Sucrose solution 100 mL

30g sucrose
100 mL 0.125M PB

Dissolve the sucrose in PB.

Ethanol baths used in Nissl Staining

70%: 700 mL 96% ethanol + 260 mL distilled water
80%: 500 mL 96% ethanol + 100 mL distilled water
90%: 800 mL 96% ethanol + 50 mL distilled water

Ethanol/acetic acid

500 mL ethanol (70%)
2.5 mL acetic acid

Cresyl Violet

0.5g Cresyl violet
500 mL

Appendix VI: List of Chemicals and Antibodies

Primary antibodies and secondary antibodies	Manufacturer
Goat anti-somatostatin	Santa Cruz Biotechnology
Rabbit anti-green fluorescent protein (GFP)	Invitrogen
Mouse anti-mCherry	Clontech
Rat anti-HA tag	(Sigma) Roche
Normal Goat Serum	Abcam
Normal Donkey Serum	Sigma
Goat anti-mouse AF546	Invitrogen
Goat anti-rat AF488	Invitrogen
Goat anti-rat AF546	Invitrogen
Goat anti-rabbit AF 488	Invitrogen
Donkey anti-goat AF546	Invitrogen

Chemicals	Manufacturer
Acetic Acid	VWR
Cresyl Violet	Sigma-Aldrich
Dimethyl sulfoxide (DMSO)	VWR
Entellan	Merck
Ethanol	Kemetyl Norge A/S
Glycerine	VWR
Hydrogen chloride (HCl)	Merck
Paraformaldehyde	Merck
Phosphate Buffer (PB)	Merck
Potassium chloride (KCl)	Merck
Sodium chloride (NaCl)	VWR
Sodium bicarbonate (NaHCO3)	Merck
Sucrose	VWR
Toluene	VWR
Tris (hydroxmethyl) aminomethane	Merck
Triton X-100	Merck
Xylene	Merck